Received: 3 October 2019 | Revised: 2 January 2020 | Accepted: 2 January 2020

DOI: 10.1002/aoc.5508

FULL PAPER

Applied Organometallic Chemistry WILEY

# Synthesis and characterization of dimeric μ-oxidovanadium complexes as the functional model of vanadium bromoperoxidase

**Abhishek Maurya**[1] | **Arun Kumar Mahato**[1] | **Nikita Chaudhary**[2] | **Neha Kesharwani**[1] | **Payal Kachhap**[1] | **Vivek Kumar Mishra**[1] | **Chanchal Haldar**[1]

[1]Department of Chemistry, Indian Institute of Technology (Indian School of Mines), Dhanbad, 826004, Jharkhand, India

[2]Department of Chemistry and Polymer Science, Stellenbosch University, Matieland, 7602, Stellenbosch, South Africa

**Correspondence**
Chanchal Haldar, Department of Chemistry, Indian Institute of Technology (Indian School of Mines), Dhanbad 826004, Jharkhand, India.
Email: chanchal@iitism.ac.in

**Funding information**
Science and Engineering Research Board, Grant/Award Number: SB/EMEQ-055/2014

Two vanadium (IV) complexes $[V^{IV}O(Haeae\text{-}sal)(MeOH)]^+$ (**1**) and $[V^{IV}O(Haeae\text{-}hyap)(MeOH)]^+$ (**2**) were prepared by reacting $[VO(acac)_2]$ with ligands $[H_2aeae\text{-}sal]$ (**I**) and $[H_2aeae\text{-}hyap]$ (**II**) respectively. Condensation of 2-(2-aminoethylamino)ethanol with salicylaldehyde and 2-hydroxyacetophenone produces the ligands (**I**) and (**II**) respectively. Both vanadium complexes **1** and **2** are sensitive towards aerial oxygen in solution and rapidly convert into vanadium(V) dioxido species. Vanadium(V) dioxido species crystalizes as the dimeric form in the solid-state. Single-crystal XRD analysis suggests octahedral geometry around each vanadium center in the solid-state. To access the benefits of heterogeneous catalysis, vanadium(V) dioxido complexes were anchored into the polymeric chain of chloromethylated polystyrene. All the synthesized neat and supported vanadium complexes have been studied by a number of techniques to confirm their structural and functional properties. Bromoperoxidase activity of the synthesized vanadium(V) dioxido complexes **3** and **4** was examined by carrying out oxidative bromination of salicylaldehyde and oxidation of thioanisole. In the presence of hydrogen peroxide, **3** shows 94.4% conversion **(**TOF value of $2.739 \times 10^2\ h^{-1}$) and **4** exhibits 79.0% conversion (TOF value of $2.403 \times 10^2\ h^{-1}$) for the oxidative bromination of salicylaldehyde where 5-bromosalicylaldehyde appears as the major product. Catalysts **3** and **4** also efficiently catalyze the oxidation of thioanisole in the presence of hydrogen peroxide where sulfoxide is observed as the major product. Covalent attachment of neat catalysts **3** and **4** into the polymer chain enhances substrate conversion (%) and their catalytic efficiency increases many folds, both in the oxidative bromination and oxidation of thioether. Polymer supported catalysts **5** displayed 98.8% conversion with a TOF value of $1.127 \times 10^4\ h^{-1}$ whereas catalyst **6** showed 95.7% conversion with a TOF value of $4.675 \times 10^3\ h^{-1}$ for the oxidative bromination of salicylaldehyde. These TOF values are the highest among the supported vanadium catalysts available in the literature for the oxidative bromination of salicylaldehyde.

  

**KEYWORDS**

elemental mapping, heterogeneous catalysis, single crystal XRD, vanadium bromoperoxidase model, μ-oxidovanadium complexes

## 1 | INTRODUCTION

The field of the coordination chemistry of vanadium is becoming a popular choice among the researchers gradually. Vanadium and its complexes are found to be an active component in various biological processes like haloperoxidation,[1] phosphorylation,[2] nitrogen fixation,[3] glycogen metabolism,[4] and insulin mimicking.[5] Especially, the appearance of vanadium in the active site of vanadium haloperoxidases[1] and its active involvement in the various important catalytic reactions[6] has encouraged participation in the research of coordination chemistry of vanadium. Vanadium bromoperoxidase, isolated from marine algae and fungus, is the most discussed member in the vanadium dependent enzymes,[6b] which is actively involved in the biosynthesis of brominated natural products. Vanadium bromoperoxidase promotes the oxidation and oxidative bromination of organic compounds in the presence of hydrogen peroxide or molecular oxygen.[7] During the catalytic cycle, in situ generated peroxido vanadium(V) is believed to be the active species responsible for the catalytic oxidation of bromide where a change in geometry between trigonal bipyramidal and square pyramidal is suggested by X-ray crystallography.[8] Hence, to understand the structural and functional behavior of vanadium in biological systems, fundamental research on vanadium oxo complexes with various oxidation states such as +3, +4 and + 5 has become essential. Because of higher stability and tunable electronic environment, vanadium(V) complexes are frequently developed as the structural and functional models of vanadium haloperoxidase.[9] In association with catalytic oxidation of halides, the mononuclear vanadium cofactor[10] is capable of accelerating the oxidation of organic sulfides to sulfoxides and sulfones in the presence of hydrogen peroxide.[11] Besides these, vanadium complexes are found to catalyze a number of oxidative organic transformations like alcohol oxidation, oxidation of hydrocarbons, halide oxidation, etc.[12]

There is a steady demand for organobromines in the area of organic synthesis and the chemical industry.[13] Organobromine compounds are applied in various fields such as materials,[14] flame retardants, emulsifiers,[15] agrochemicals, pharmaceuticals,[16] and intermediates which makes them one of the important classes of compounds in our society. Despite the hazardous nature of liquid molecular bromine, it is used for the production of a large fraction of industrial and chemical organobromine compounds.[17] Molecular bromine is a toxic, volatile and corrosive chemical that restricts its use as a brominating agent. Whereas, the formation of in situ bromine from the oxidation of bromide by oxygen or hydrogen peroxide is much more economical and green. But surprisingly at normal pH, the oxidation of bromide by peroxides is very slow. Nature uses vanadium bromoperoxidase to catalyze the oxidation of bromide in the presence of hydrogen peroxide.

Herein, we report two new vanadium (IV) oxido complexes $[V^{IV}O(Haeae\text{-}sal)(MeOH)]^+$ (**1**) and $[V^{IV}O(Haeae\text{-}hyap)(MeOH)]^+$ (**2**) of Schiff-base $[H_2aeae\text{-}sal]$ (**I**) and $[H_2aeae\text{-}hyap]$ (**II**). Upon dissolution, in the presence of air, these complexes spontaneously convert into the corresponding vanadium(V) dioxido complexes. In 1988 Li et al. first reported the structure and electrochemical properties of the complex $[\{V^{V}O(Haeae\text{-}sal)\}\mu\text{-}O]_2$ (**3**), and later in 2010 Xie et al. reported its antidiabetic properties, whereas In 2013 Zhao et al. reported the structure and antimicrobial properties of the complex $[\{V^{V}O(Haeae\text{-}hyap)\}\mu\text{-}O]_2$ (**4**).[18] But none of the research papers focused on the structural uniqueness of the complexes $[\{V^{V}O(Haeae\text{-}sal)\}\mu\text{-}O]_2$ (**3**) and $[\{V^{V}O(Haeae\text{-}hyap)\}\mu\text{-}O]_2$ (**4**) and examined their catalytic potential. Single-crystal XRD analysis suggests that both the complexes **3** and **4** exist in the dimeric form in solid-state where each vanadium center adopts an octahedral geometry. We have observed that in solution both vanadium(V) complexes exist in the monomeric form where the vanadium center acquires a geometry similar to the active form of vanadium haloperoxidase, which convinced us to use them as functional models of vanadium bromopeoxidase. Thus complexes $[\{V^{V}O(Haeae\text{-}sal)\}\mu\text{-}O]_2$ (**3**) and $[\{V^{V}O(Haeae\text{-}hyap)\}\mu\text{-}O]_2$ (**4**) have been applied towards the catalytic oxidation of bromide and sulfide. Oxidative bromination of salicylaldehyde in the presence of reported catalysts proceeds with high substrate conversion (%) and TOF values. To make the catalytic process more green, economic and for easy catalyst separation, heterogeneous catalysts were developed by covalent anchoring of the neat catalysts into the polymeric chain of chloromethylated polystyrene. Heterogenization enhances the substrate conversion (%) as well as the TOF values greatly. Hence we present the synthesis, detailed characterization, and catalytic activity of the neat and polymer anchored vanadium(V)

complexes towards the oxidative bromination of salicylaldehyde and oxidation of thioanisole in the presence of hydrogen peroxide.

## 2 | EXPERIMENTAL

### 2.1 | Materials

Analytical grade reagent $V_2O_5$ (Loba Chemie, Mumbai, India), acetylacetone (Merck, India), 2-(2-aminoethylamino) ethanol (Alfa-Aesar, Mumbai, India), salicylaldehyde (SRL, India), 2-hydroxyacetophenone (Loba Chemie, Mumbai, India), chloromethylated polystyrene (1% cross-linked with divinylbenzene 50–100 mesh, extent of labeling: 2.5–4.0 mmole/g $Cl^-$ loading) (Sigma-Aldrich, New Mumbai, India), Nujol (paraffin wax heavy oil, SRL, India), KI (Rankem, Thane, India), 30% aqueous $H_2O_2$ (Merck, Mumbai, India), 70% $HClO_4$ (Rankem, Thane, India) and thioanisole (Alfa-Aesar, Mumbai, India) were used as obtained. Other chemicals and solvents were of analytical reagent grade. HPLC grade solvents (Spectrochem, Mumbai, India) were used for GC and GC–MS analysis. $[V^{IV}O(acac)_2]$[19] was prepared according to the reported method.

### 2.2 | Physical methods and analysis

Elemental analysis was carried out by Electron Probe Microanalyser SX, CAMECA (France) instrument. FT-IR spectra were recorded in ATR mode by using Agilent 600 series FT-IR spectrophotometer. Electronic spectra were measured in a Shimadzu UV-1800 spectrophotometer using methanol as a solvent. Nujol was used for recording the electronic spectra of polymer-bound metal complexes. $^1$H NMR spectra of the ligands were recorded in $CDCl_3$ and $^{13}$C NMR spectra of the ligands were recorded in DMSO-$d_6$ solvent on a Bruker Avance II 400 MHz NMR spectrometer with the common parameter settings. $^{51}$V NMR spectra of vanadium(V) oxido complexes were recorded in a JEOL-ECZ 500 MHz spectrometer at 131.55 MHz frequency in DMSO-$d_6$ by using $VOCl_3$ as an external standard. The X-band EPR of vanadium (IV) complexes were recorded in methanol with a JES-FA200 spectrometer operating at 100 kHz at liquid nitrogen temperature.

Elemental mapping and surface morphology of polymer anchored vanadium complexes were analyzed by Energy Dispersive X-ray Analysis (EDX) and scanning electron microscope (SEM) on a Hitachi S-3400 N instrument after coating the polymer bead surface with a thin film of gold to block the surface charging and thermal damage by the electron beam. Vanadium content was estimated by Lab India, AA 8000 atomic absorption spectrometer, after digesting the polymer-bound metal complexes by conc. $HNO_3$ and subsequent diluting the filtrate. For AFM imaging of polymers, a scanning probe microscope from DIMENSION iCON with ScanAsyst was used. Thermogravimetric analysis (TGA) was performed by using Perkin Elmer, Diamond TG/DTA instrument. An Agilent 7890 B gas-chromatograph fitted with an HP-5 capillary column (30 m × 0.25 mm × 0.25 μm) and an FID detector was used to analyze the reaction products. Substrate conversion (%) was calculated using the calibration plot. The identity of the oxidation products was confirmed by Thermo ISQ QD single quadrupole mass analyzer. Substrate conversion (%) and product selectivity (%) were calculated by using the following formulae:

$$\text{Substrate Conversion}\,(\%) = 100 - \frac{\textit{Area of substrate}}{\textit{Total area of substrate} + \textit{Area of products}} \times 100, \quad (1)$$

$$\text{Similarly, product selectivity}\,(\%) = 100 - \frac{\textit{Area of product}}{\textit{Total area of products}} \times 100,$$

### 2.3 | Computational method

Gaussian 09[20] program pack was used to perform all the theoretical calculations with the help of an HP Z440 work station. For visualization, GaussView 5.0[21] and Chemcraft[22] molecular graphical programs were used. X-ray refinement data were taken as an initial gauss for the optimization of the molecular structures. The solution phase and gas phase molecular structure of the ligands and metal complexes in the ground state was optimized by Density Functional Theory (DFT) in its restricted and unrestricted forms, without any symmetry constraint. All the calculations were carried out with 6-31G (d,p)[23,24] basis set for the C, H, N, O elements and DFT/UB3LYP employing LANL2DZ basis set with an effective core potential for the V atom.[25] In the DFT calculation, hybrid functional was also used. The Becke's three-parameter functional (B3)[26] was used in combination with the correlation functional of Lee et al.[27] Density functional theory was used to evaluate the chemical reactivity and some selective global parameters such as electronegativity ($\chi$) hardness ($\eta$) and softness ($\sigma$) Thus for an electron system with total electronic energy (E) and an external potential V(r), chemical potential ($\rho$) is known as the first derivative of the E with respect to N at V(r).[28]

$$\begin{aligned}\chi &= \rho \\ &= -(\partial E/\partial N))\zeta(\rho)\end{aligned} \quad (2)$$

Hardness (η) has been defined as the second derivative of the E with respect to N at V(r) property, which measures both the stability and reactivity of a molecule.[29]

$$= -\left(\partial^2 E/\partial N^2\right)\varsigma(\rho) = -(\partial\rho/\partial N)\varsigma(\rho) \quad (3)$$

Where E is the electric energy, N is the number of electrons and V(r) is the external potential due to the nuclei and ρ is chemical potential. For the compounds **3**, **3(a)**, **4**, and **4(a)** vibrational frequencies were calculated by using DFT/UB3LYP/6-31G (d) level of theory. Lack of Imaginary frequency confirms the optimized structure as local minima in the potential energy surface.

## 3 | CATALYTIC ACTIVITY

### 3.1 | Oxidative bromination of salicylaldehyde

Oxidative bromination of salicylaldehyde was carried out at room temperature. Conventionally, salicylaldehyde (10 mmol, 1.22 g) was reacted with 30% aqueous dilute $H_2O_2$ (15 mmol, 1.70 g), 70% aqueous $HClO_4$ (20 mmol, 2.86 g) and KBr (20 mmol, 2.38 g) in the presence of a polymer-supported catalyst in 20 ml of water at room temperature. The reaction continued for two hours while precipitate separates from the solution. By using DCM as a solvent, unreacted substrate and brominated products were isolated from the reaction mixture by solvent extraction. Substrate conversion (%) and product selectivity (%) were estimated by analyzing the DCM extract on a Gas Chromatography. To improve the catalytic efficiency addition of perchloric acid in three equal portions with a fixed time interval (15 min) is necessary. The identities of the brominated products were confirmed by the available external commercial standards as well as GC–MS.

### 3.2 | Oxidation of Thioanisole

Oxidation of thioanisole was catalyzed by **5** and **6** at room temperature. In a typical reaction, thioanisole (5 mmol, 0.627 g) and 30% $H_2O_2$ (12.5 mmol, 1.417 g) were reacted in the presence of 0.020 g pre-swelled (in 4 ml acetonitrile for 6 hr) catalyst with constant stirring for 4 hr at room temperature. Periodically a small aliquot was withdrawn from the reaction mixture and analyzed quantitatively through a Gas Chromatograph. The impact of different parameters on this reaction such as time, amounts of catalyst, amounts of oxidant, amounts of solvent (acetonitrile), and nature of solvents were monitored and optimized to get the efficient oxidative desulfurization of thioanisole. Identities of the reaction products were confirmed from GC–MS analysis.

### 3.3 | X-ray crystallography

The data of complexes $[\{VO^V(Haeae\text{-}sal)\}\mu\text{-}O]_2$ (**3**) and $[\{VO^V(Haeae\text{-}hyap)\}\mu\text{-}O]_2$ (**4**) were collected by Rigaku Oxford Diffraction system equipped with state of the art CCD Eos S2 detector using Mo K\α radiation (wavelength 0.71073 Å) at room temperature. The data collection and reduction were executed with the Oxford diffraction Crysalis system. The structures of complexes **3** and **4** were solved by direct methods (SIR92)[30] and refined on $F^2$ by full-matrix least-squares methods employing SHELXS–2013 and SHELXL–2013 programs.[30,31] The molecular graphics were haggard using the PLATON program. Non-hydrogen atoms(C, O, N, and V) were anisotropically refined. All H atoms were put in calculated location riding on their carrier atoms. The function minimized was $[\Sigma w (F_o^2 - F_c^2)^2]$ $(w = 1/[\sigma^2(F_o^2) + (aP)^2 + bP])$, where $P = (Max (F_o^2,0) + 2F_c^2)/3$ with $\sigma^2(F_o^2)$ from counting statistics. The function $R_1$ and $wR_2$ were $(\sigma||F_o|-|F_c||)/\sigma|F_o|$and $[\sigma w (F_o^2-F_c^2)^2/\sigma (wF_o^4)]^{1/2}$, respectively. CCDC No. 1957124 for complex **4** contains the supplementary crystallographic data for this paper. The crystallographic details are summarized in Table 1 and Table S1.

## 4 | SYNTHETIC PROCEDURES

### 4.1 | Preparation of ligands [$H_2$aeae-sal] (I) and [$H_2$aeae-hyap] (II)

Both ligands [$H_2$aeae-sal] (**I**) and [$H_2$aeae-hyap] (**II**) were prepared according to the method shown in Scheme 1. In short, 20 ml methanolic solution of 2-(2-aminoethylamino)ethanol (10 mmol, 1.04 g) was added dropwise into 20 ml methanolic solution of salicylaldehyde (10 mmol, 1.22 g) or 2-hydroxyacetophenone (10 mmol, 1.36 g) with constant stirring. The resulting reaction mixture was refluxed for 2 hr. The progress of the reaction was checked by TLC. After 2 hr, the volume of the resulting yellow reaction mixture was reduced to ~15 ml and kept in a refrigerator overnight. The yellow precipitate thus obtained was filtered, washed with cold methanol (2 × 5 ml) followed by petroleum ether and dried over silica gel under vacuum.

**TABLE 1** Crystal and refinement parameters for complexes **4**

| Identification code | (4) |
|---|---|
| Empirical formula | $C_{24}H_{34}N_4O_8V_2$ |
| Formula weight | 608.44 |
| Temperature/K | 293(2) |
| Crystal system | Monoclinic |
| Space group | P 21/c |
| a(Å) | 11.2062(9) |
| b(Å) | 11.0681(10) |
| c(Å) | 11.0883(8) |
| α(°) | 90.000 |
| β(°) | 109.950(9) |
| γ(°) | 90.000 |
| Volume (Å$^3$) | 1292.8(2) |
| Z | 2 |
| ρcalc (g cm$^{-3}$) | 1.5629 |
| μ (mm$^{-1}$) | 0.779 |
| F(000) | 633.6 |
| Crystal size/mm$^3$ | 0.15 × 0.12 × 0.1 |
| Radiation Mo Kα (λ) | 0.71073 |
| 2θ range for data collection (°) | 3.86 to 54.00 |
| Index ranges | −15 ≤ h ≤ 12, −14 ≤ k ≤ 15, −9 ≤ l ≤ 14 |
| Reflections collected | 6207 |
| Independent reflections | 2768 [Rint = 0.0254, Rsigma = 0.0428] |
| Data/restraints/parameters | 2768/0/173 |
| Goodness-of-fit on F$^2$ | 1.0553 |
| Final R indexes $R_1(I > 2\sigma(I))$, $wR_2$ | 0.0376, 0.0781 |
| Final R indexes [all data] $R_1$, $wR_2$ | 0.0584, 0.0866 |
| Largest diff. Peak/hole/e Å$^{-3}$ | 0.42/−0.43 |

### 4.1.1 | Data for [$H_2$aeae-sal] (I)

Compound isolated 1.98 g (yield 95.5%). Anal. calcd. For $C_{11}H_{16}N_2O_2$ (M.W. 208.26): C, 63.44%; H, 7.74%; N, 13.45%. Found: C, 63.55%; H, 7.80%; N, 13.51%. FT-IR (ATR method, cm$^{-1}$): 3444($\nu_{OH}$), 3300($\nu_{N\text{-}H}$), 1626($\nu_{C=N}$), 1295($\nu_{C\text{-}O}$). UV–Vis [$\lambda_{max}$ (nm), ε (Lmol$^{-1}$ cm$^{-1}$)]: 400 (8.63 × 10$^2$), 315 (3.38 × 10$^3$), 280 (2.60 × 10$^3$), 255 (1.03 × 10$^4$), 215 (2.09 × 10$^4$). $^1$H NMR ($CDCl_3$, δ in ppm): 8.33(s, 1H), 7.26–7.30(dt, 1H), 7.21–7.23(dd, 1H), 6.91–6.93(d, 1H), 6.83–6.87(dt, 1H), 3.68(t, 2H), 3.60–3.63(t, 2H), 2.91–2.94(t, 2H), 2.74–2.76(t, 2H). $^{13}$C-NMR (DMSO-$d_6$, δ in ppm): 166.52, 161.09, 132.27, 131.66, 118.87, 118.45, 116.76, 60.42, 58.57, 51.78, 49.84.

### 4.1.2 | Data for [$H_2$aeae-hyap] (II)

Compound isolated 2.13 g (yield 95.94%). Anal. calcd. For $C_{12}H_{18}N_2O_2$ (M.W. 222.28): C, 64.84%; H, 8.16%; N, 12.60%. Found: C, 64.78%; H, 8.18; N,12.69%. FT-IR (ATR method, cm$^{-1}$): 3419($\nu_{OH}$), 3293($\nu_{N\text{-}H}$), 1609($\nu_{C=N}$), 1299($\nu_{C\text{-}O}$). UV–Vis [$\lambda_{max}$ (nm), ε (Lmol$^{-1}$ cm$^{-1}$)]: 390 (3.28 × 10$^3$), 324 (2.43 × 10$^3$), 272 (6.22 × 10$^3$), 255 (7.46 × 10$^3$), 216 (2.04 × 10$^4$). $^1$H NMR ($CDCl_3$, δ in ppm): 16.44(s, b), 7.52–7.54(d, 1H), 7.22–7.26(t, 1H), 6.79–6.81(d, 1H), 6.71–6.74(t, 1H), 3.67–3.70(t, 2H), 3.59–3.61(t, 2H), 2.98–3.01(t, 2H), 2.75–2.78(t, 2H), 2.38(s, 3H). $^{13}$C-NMR (DMSO-d6, δ in ppm): 173.22, 165.35, 132.86, 128.98, 118.95, 118.65, 116.33, 60.57, 51.71, 49.46, 48.68, 14.52.

## 5 | SYNTHESIS OF VANADIUM COMPLEXES

### 5.1 | Preparation of [$V^{IV}$O(Haeae-sal)(MeOH)]$^+$ (1)

Deaerated 20 ml methanolic solution of [$H_2$aeae-sal] (**I**) (10 mmol, 2.08 g) was mixed with deaerated 30 ml

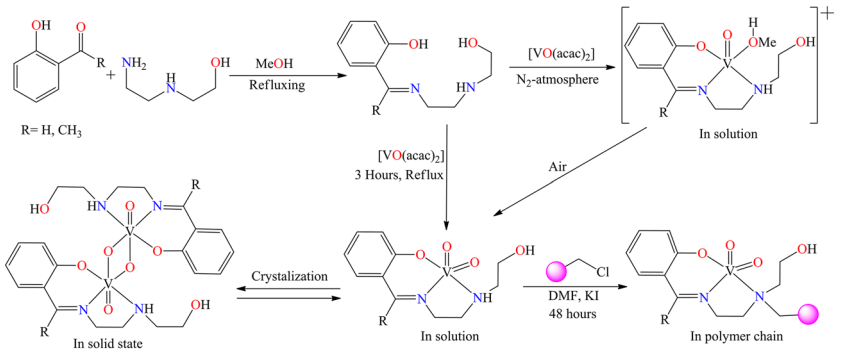


**SCHEME 1** Synthetic scheme for the preparation of ligands and metal complexes along with the heterogenization of vanadium complexes

methanolic solution of [VO (acac)$_2$] (2.65 g) under a nitrogen atmosphere with constant stirring. The reaction mixture was refluxed for one hour. Afterward, the brown-colored solution was reduced to dryness under vacuum, during which a light brown colored compound **1** was separated which was filtered off, washed with methanol and finally dried under vacuum.

### 5.1.1 | Data for [$V^{IV}$O(Haeae-Sal)(MeOH)]$^+$ (1)

Yield 2.45 g (80.01%). Anal. calcd. For $C_{12}H_{19}N_2O_4V$ (M. W. 306.23): C, 47.07%; H, 6.25%; N, 9.15% Found: C, 47.38%; H, 6.50; N, 9.05%. FT-IR (ATR method, $cm^{-1}$): 3397($\nu_{OH}$), 3210($\nu_{N\text{-}H}$), 1591($\nu_{C=N}$), 1278($\nu_{C\text{-}O}$), 936($\nu_{V=O}$). UV–Vis [$\lambda_{max}$ (nm), $\varepsilon$ ($Lmol^{-1}$ $cm^{-1}$)]: 802 (20), 372 (3.39 × $10^3$), 272 (1.92 × $10^4$), 232 (2.47 × $10^4$).

Using a similar method, complex [$V^{IV}$O(Haeae-hyap)(MeOH)]$^+$ (**2**) was isolated by reacting [VO (acac)$_2$] (10 mmol, 2.65 g) with [$H_2$aeae-hyap] (**II**) (10 mmol, 2.22 g) in deaerated methanol under nitrogen atmosphere.

### 5.1.2 | Data for [$V^{IV}$O(Haeae-hyap)(MeOH)]$^+$ (2)

Yield 2.674 g (83.49%). Anal. calcd. For $C_{13}H_{21}N_2O_4V$ (M. W. 320.26): C, 48.75%; H, 6.61%; N, 8.75%. Found: C, 48.88%; H, 6.85; N, 8.65%. FT-IR (ATR method, $cm^{-1}$): 3368($\nu_{OH}$), 3289($\nu_{N\text{-}H}$), 1576($\nu_{C=N}$), 1234($\nu_{C\text{-}O}$), 936($\nu_{V=O}$). UV–Vis [$\lambda_{max}$ (nm), $\varepsilon$ ($Lmol^{-1}$ $cm^{-1}$)]: 786 (28), 372 (8.10 × $10^2$), 305 (3.97 × $10^4$), 272 (5.38 × $10^4$), 231 (5.61 × $10^4$).

### 5.1.3 | Preparation of [{$V^{V}$O(Haeae-sal)}μ-O]$_2$ (3) and [{$V^{(V)}$O(Haeae-hyap)}μ-O]$_2$ (4)

Method A: 30 ml methanolic solution of [VO (acac)$_2$] (10 mmol, 2.65 g) was reacted with 15 ml methanolic solution of [$H_2$aeae-sal] (**I**) (10 mmol, 2.08 g) or [$H_2$aeae-hyap] (**II**) (10 mmol, 2.22 g) with constant stirring at room temperature and pressure. The solution was refluxed for 3 hr in the presence of air. After 3 hr, the reddish-brown colored solution was reduced to ~15 ml and kept in a refrigerator overnight. Within 4–5 days, light orange colored crystals suitable for X-ray analysis were isolated from the solution.

Method B: 5.0 mmol (1.53 g) [$V^{IV}$O(Haeae-sal)(MeOH)]$^+$ (**1**) or 5.0 mmol (1.60 g) [$V^{IV}$O(Haeae-hyap)(MeOH)]$^+$ (**2**) was dissolved in the minimum amount of DMSO (10 ml) and kept for slow evaporation in the open air. Within 6–8 days, crystals suitable for X-ray analysis appeared in the solution.

### 5.1.4 | Data for [{$V^{V}$O(Haeae-sal)}μ-O]$_2$ (3)

Yield 0.819 g (30%). Anal. calcd. For $C_{22}H_{30}N_4O_8V_2$ (M. W. 580.39): C, 45.53%; H, 5.21%; N, 9.65%. Found: C, 45.48%; H, 5.42%; N, 9.55%. FT-IR (ATR method, $cm^{-1}$): 3397($\nu_{OH}$), 3211($\nu_{N\text{-}H}$), 1597($\nu_{C=N}$), 1276($\nu_{C\text{-}O}$), 937($\nu_{V=O}$), 770($\nu_{V\text{-}(\mu\text{-}O)\text{-}V}$)$_{asymmetric}$, 840($\nu_{V\text{-}(\mu\text{-}O)\text{-}V}$)$_{symmetric}$. UV–Vis [$\lambda_{max}$ (nm), $\varepsilon$ ($Lmol^{-1}$ $cm^{-1}$)]: 385 (1.84 × $10^3$), 316 (5.97 × $10^3$), 277 (1.21 × $10^4$), 254 (2.15 × $10^4$), 215 (4.36 × $10^4$).

### 5.1.5 | Data for [{$V^{(V)}$O(Haeae-hyap)}μ-O]$_2$ (4)

Yield 1.022 g (35.6%). Anal. calcd. For $C_{24}H_{34}N_4O_8V_2$ (M. W. 608.44): C, 47.48%; H, 5.63%; N, 9.21%. Found: C, 47.43%; H, 5.79%; N, 9.15%. FT-IR (ATR method, $cm^{-1}$): 3374($\nu_{OH}$), 3271($\nu_{N\text{-}H}$), 1581($\nu_{C=N}$), 1233($\nu_{C\text{-}O}$), 932($\nu_{V=O}$), 743($\nu_{V\text{-}(\mu\text{-}O)\text{-}V}$)$_{asymmetric}$, 822($\nu_{V\text{-}(\mu\text{-}O)\text{-}V}$)$_{symmetric}$. UV–Vis [$\lambda_{max}$ (nm), $\varepsilon$ ($Lmol^{-1}$ $cm^{-1}$)]: 387 (1.70 × $10^3$), 321 (1.10 × $10^4$), 276 (1.22 × $10^4$), 250 (3.83 × $10^4$), 212 (7.95 × $10^4$).

## 5.2 | Synthesis of polymer-supported vanadium complexes

Preparation of PS-[$V^{V}O_2$(Haeae-sal)] (**5**) and PS-[$V^{V}O_2$(Haeae-hyap)] (**6**): Covalent attachment of [{$V^{V}$O(Haeae-sal)}μ-O]$_2$ (**3**) and [{$V^{V}$O(Haeae-hyap)}μ-O]$_2$ (**4**) into the chloromethylated polystyrene bead was done by a conventional procedure described in Scheme 1. In brief, chloromethylated polystyrene (1.0 g) was allowed to swell in DMF (20 ml) for 12 hours. DMF solution (40 ml) of **3** (6.89 mmol, 4.0 g) or **4** (6.57 mmol, 4.0 g) was added to the above suspension in the presence of KI (6.69 mmol, 1.11 g) and triethylamine (2.19 gm). The reaction mixture was heated at 90 °C for 48 hr with gentle stirring (150 RPM) in an oil bath fitted with a water-cooled condenser. The cooled reaction mixture was filtered and washed with hot DMF (4 × 20 ml) followed by hot methanol (4 × 20 ml). The brown-colored polymer-

supported complex **5** or **6** was recovered and dried in a hot air oven at *ca.* 110 °C for 24 hr.

### 5.2.1 | Data for PS-[$V^{V}O_2$(Haeae-sal)] (5)

Recovery yield 96%. FT-IR (ATR method, $cm^{-1}$): 3390($\nu_{OH}$), 1587($\nu_{C=N}$), 1261($\nu_{C-O}$), 953($\nu_{V=O}$), 907($\nu_{V=O}$); UV–Vis [$\lambda_{max}$ (nm)]: 230, 264, 304, 340.

### 5.2.2 | Data for PS-[$V^{(V)}O_2$(Haeae-hyap)] (6)

Recovery yield 94.8%. FT-IR (ATR method, $cm^{-1}$): 3393($\nu_{OH}$), 1587($\nu_{C=N}$), 1212($\nu_{C-O}$), 975($\nu_{V=O}$), 904($\nu_{V=O}$); UV–Vis [$\lambda_{max}$ (nm)]: 220, 263, 312, 341 nm.

## 6 | RESULT AND DISCUSSION

### 6.1 | Electronic spectral studies

Electronic spectral data of all the ligands and metal complexes are enlisted in Table 2 and spectra are shown in Figure S1. Absorbance bands appearing in the range of 215–216 nm for both ligands **I** and **II** are due to σ-σ* transition. Both ligands show absorbance bands in the range of 255–272 nm because of π-$\pi_1$* and π-$\pi_2$* transition whereas two low-intensity absorbance bands in the range of 315–400 nm can be assigned to $n_1$-$\pi^*$ and $n_2$-$\pi^*$ transition. All these electronic transitions also appeared in the corresponding vanadium complexes with slight shifting from their original position. Additionally, $[V^{IV}O(aeae\text{-}sal)(MeOH)]^+$ (**1**) and $[V^{IV}O(aeae\text{-}hyap)(MeOH)]^+$ (**2**) exhibits a broad band, of low intensity and low energy, at 802 nm ($\varepsilon = 20\ Lmol^{-1}\ cm^{-1}$) and 786 nm ($\varepsilon = 28\ Lmol^{-1}\ cm^{-1}$), respectively, which can be assigned to *d-d* transition. The polymer anchored vanadium complexes **5** and **6** displayed low-intensity absorbance bands because of the low concentration of **3** and **4** in the polymer matrix. However, both **5** and **6** showed absorbance bands characteristic of their respective ligands (Figure S2), which confirms successful attachment of the vanadium complexes in the chloromethylated polystyrene chain.

### 6.2 | Solution behaviour of $[V^{IV}O(aeae\text{-}Sal)(MeOH)]^+$ (1) and $[V^{IV}O(aeae\text{-}hyap)(MeOH)]^+$ (2)

Both vanadium (IV) complexes 1 and 2 are stable in the solid-state but in solution, they spontaneously oxidize in the presence of aerial oxygen and quickly convert into vanadium(V) dioxido species. Absorbance spectra of the methanolic solution of 1 ($1.165 \times 10^{-2}$ M) and 2 ($2.132 \times 10^{-2}$ M) were recorded periodically (intervals of 2 minutes) in the presence of air at room temperature and pressure while stirring the solution continuously. A representative plot of change in absorbance spectra of **2** due to the aerial oxidation is shown in Figure 1. It is observed that the broad bands at 802 nm in **1** and 786 nm in **2** gradually disappear with time (Figure 1 and

**TABLE 2** Electronic spectral data of the ligands and their vanadium complexes

| SN | Compound | Solvent | $\lambda_{max}$ (nm) /(ε)($Lmol^{-1}\ cm^{-1}$) |
|---|---|---|---|
| 1 | [$H_2$aeae-sal] (**I**) | MeOH | 400($8.63 \times 10^2$), 315($3.38 \times 10^3$), 280(sh), 255($1.03 \times 10^4$), 215($2.09 \times 10^4$) |
| 2 | [$H_2$aeae-hyap] (**II**) | MeOH | 390($3.28 \times 10^3$), 324($2.43 \times 10^3$), 272($6.22 \times 10^3$), 255($7.46 \times 10^3$),216($2.04 \times 10^4$) |
| 3 | $[VO^{IV}$(Haeae-sal)(MeOH)]$^+$ (**1**) | MeOH | 802(20)$^{\$}$, 372($3.39 \times 10^3$), 272($1.92 \times 10^4$), 232($2.47 \times 10^4$) |
| 4 | $[VO^{IV}$(Haeae-Hyap)(MeOH)]$^+$ (**2**) | MeOH | 786(28)$^{\$}$, 372($8.10 \times 10^2$), 305($3.97 \times 10^4$), 272($5.38 \times 10^4$), 231($5.61 \times 10^4$) |
| 5 | [{$VO^{V}$(Haeae-sal)}μ-O]$_2$ (**3**) | MeOH | 385($1.84 \times 10^3$), 316($5.97 \times 10^3$), 277($1.21 \times 10^4$), 254($2.15 \times 10^4$), 215($4.36 \times 10^4$) |
| 6 | [{$VO^{V}$(Haeae-hyap)}μ-O]$_2$ (**4**) | MeOH | 387($1.70 \times 10^3$), 321($1.10 \times 10^4$), 276($1.22 \times 10^4$), 250($3.83 \times 10^4$), 212($7.95 \times 10^4$) |
| 7 | PS-[$V^{V}O_2$(Haeae-sal)] (**5**) | Nujol | 340, 304, 264, 230 |
| 8 | PS-[$V^{V}O_2$(Haeae-hyap)] (**6**) | Nujol | 341, 312, 263, 220 |

$^{\$}$= *d-d* transition.

sh = shoulder band.

Figure S3) which suggests the formation of corresponding vanadium(V) dioxido species in solution as proposed in the scheme 1.

The methanolic solution of $3.210 \times 10^{-5}$ M of $[\{VO^{V}(Haeae\text{-}sal)\}\mu\text{-}O]_2$ (**3**) and $1.550 \times 10^{-4}$ M of $[\{VO^{V}(Haeae\text{-}hyap)\}\mu\text{-}O]_2$ (**4**) was reacted with dilute aqueous hydrogen peroxide and the corresponding spectral changes are plotted in Figure 2 and Figure S4. The gradual addition of one drop portion of $8.82 \times 10^{-3}$ M (diluted in methanol) $H_2O_2$ into the methanolic solution of **3** decreases the intensities of absorbance bands at 254 nm and 316 nm, and a new band appears at 364 nm whereas the 277 nm band intensifies. Similar changes can also be seen while reacting **4** with $8.82 \times 10^{-3}$ M of hydrogen peroxide. All these changes support the generation of vanadium peroxido species in solution.

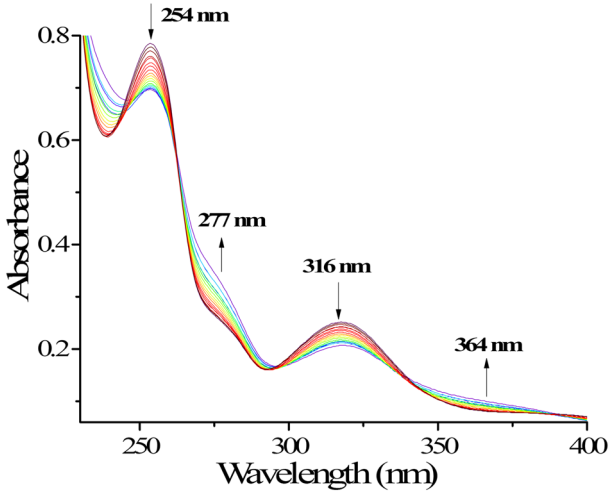


**FIGURE 2** Observed spectral changes of methanolic solution of $3.210 \times 10^{-5}$ M $[\{VO^{V}(Haeae\text{-}sal)\}\mu\text{-}O]_2$ (**3**) by the addition of methanolic solution of 1 drop portion of $8.82 \times 10^{-3}$ M dilute aqueous $H_2O_2$

## 6.3 | IR spectral studies

Changes in the functional groups, during the heterogenization of metal complexes **3** and **4** into the polymeric chain, were examined by FT-IR spectral analysis in the range of 400–4000 $cm^{-1}$. Both ligands [$H_2$aeae-sal] (**I**) and [$H_2$aeae-hyap] (**II**) display one broad $\nu_{(O\text{-}H)}$ band in the range of 3419–3444 $cm^{-1}$, the N-H stretching frequency in the range of 3293–3300 $cm^{-1}$ and one sharp band characteristic of $\nu_{(C=N)}$ in the range of 1609–1626 $cm^{-1}$. A partial list of stretching frequencies of ligands and the metal complexes of primary interest is given in Table S2. Also, selected FT-IR spectra are shown in Figure 3 and Figure S5.

Metal complexes $[V^{IV}O(aeae\text{-}sal)(MeOH)]^+$ (**1**), $[V^{IV}O(aeae\text{-}hyap)(MeOH)]^+$ (**2**), $[\{VO^{V}(Haeae\text{-}sal)\}\mu\text{-}O]_2$ (**3**) and $[\{VO^{V}(Haeae\text{-}hyap)\}\mu\text{-}O]_2$ (**4**) produce $\nu_{(O\text{-}H)}$, $\nu_{(N\text{-}H)}$ and $\nu_{(C=N)}$ stretching frequencies in their expected regions. A sharp and strong band, in the range of 932–937 $cm^{-1}$, characteristic of V=O bond is present in the FT-IR spectra of all vanadium complexes **1–4**. Moreover, all the metal complexes show slight shifting in the $\nu_{(N\text{-}H)}$ and $\nu_{(C=N)}$ stretching frequencies towards the lower wavenumber with respect to their corresponding ligands due to the coordination of amine N and azomethine N to the vanadium center.[32] Stretching frequencies in the range of 743–770 $cm^{-1}$ (in complex **3**) and 822–840 $cm^{-1}$ (in complex **4**) appear due to the symmetric and asymmetric stretching of V-O-V bond vibrations. Polymer anchored metal complexes PS-$[V^{V}O_2(Haeae\text{-}sal)]$ (**5**) and PS-$[V^{V}O_2(Haeae\text{-}hyap)]$ (**6**) revealed a similar spectral pattern to that of complexes **1** and **2**. However, both complexes exhibit two sharp stretching bands, one in the range of 953–975 $cm^{-1}$ and another in the range of 904–907 $cm^{-1}$, due to the unique $(O=V=O)_{asymmetric}$ and $(O=V=O)_{symmetric}$ bond vibrations. These bands indicate the presence of cis-$V^{V}O_2$ group in the polymer-bound vanadium complexes.[33] Absence of $\nu_{(N\text{-}H)}$ stretching frequency, in the polymer-bound metal complexes **5** and **6**, supports the covalent attachment of neat complexes (**3** and **4**) with the polymer matrix.

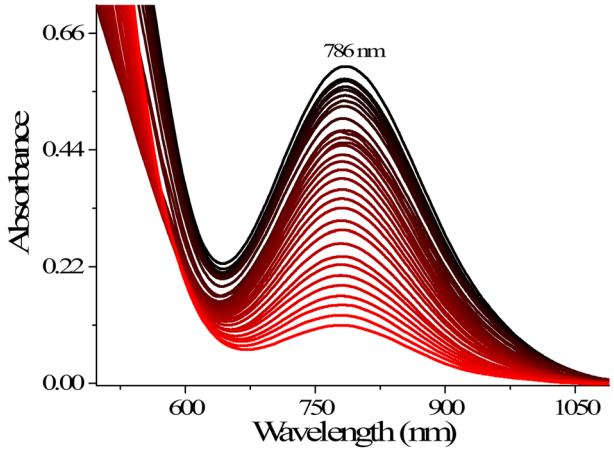


**FIGURE 1** Change in UV–Vis Spectra observed during the oxidation of 15 ml methanolic solution of $2.132 \times 10^{-2}$ M complex **2** in the presence of aerial oxygen at room temperature

## 6.4 | EPR spectral studies

The true oxidation state of vanadium (IV) oxido complexes **1** and **2** was established through EPR spectral analysis. X-band EPR spectra of complexes **1** and **2** were

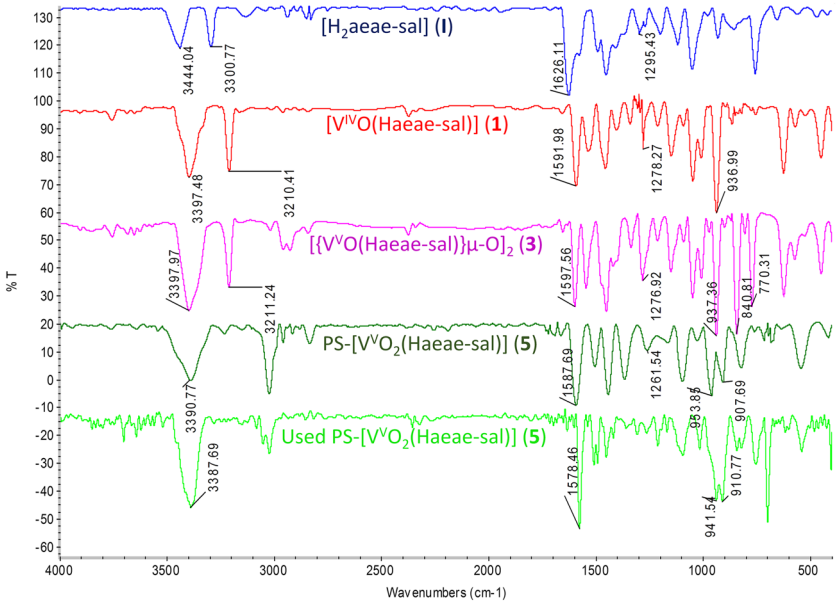


**FIGURE 3** FT-IR spectra of (A) [$H_2$aeae-sal] (**I**), [$V^{IV}$O(Haeae-sal)(MeOH)]$^+$ (**1**), [{$V^{V}$O(Haeae-sal)}μ-O]$_2$ (**3**), PS-[$V^{V}O_2$(Haeae-sal)] (**5**) and used PS-[$V^{V}O_2$(Haeae-sal)] (**5**)

recorded in methanol at liquid nitrogen temperature and presented in Figure 4.

Frozen methanolic solutions of **1** and **2** show axially symmetrical EPR spectra characteristic of $V^{(IV)}$ = O complexes.[34] A well resolved hyperfine splitting pattern, in both parallel and perpendicular regions, is observed for both of the vanadium (IV) oxido complexes **1** and **2**. Due to the coupling of one unpaired electron (S = 1/2) of $V^{4+}$ ($3d^1$) with its own nucleus (S = 7/2), 8 lines appear in the hyperfine splitting of both complexes (shown in Figure 4).

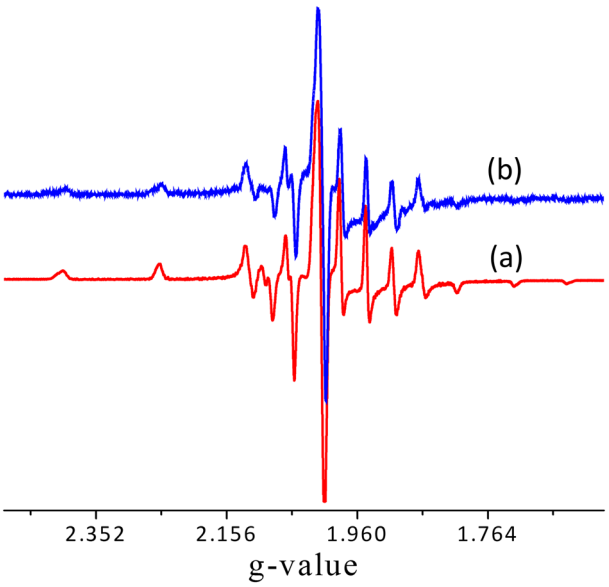


**FIGURE 4** First derivative plot of EPR spectrum of (A) [$V^{IV}$O(Haeae-sal)(MeOH)]$^+$ (**1**) and (B) [$V^{IV}$O(Haeaehyap)(MeOH)]$^+$ (**2**) recorded in methanol at 77 K. Solutions were freezed immdiately after dissolving the vanadium (IV) complexes in methanol

All the 8 lines of perpendicular orientation are clearly visible in EPR spectra of both vanadium (IV) oxido complexes but only 5 lines out of 8 in the parallel orientation are observed. However, the intensity of the spectral lines in the parallel orientation of **2** is quite low as compared to **1**. Well resolved hyperfine spectra indicate complexes **1** and **2** exist in monomeric form in the frozen methanolic solution, and mutual vanadium-vanadium interaction is absent.

## 6.5 | NMR spectral studies

$^1$H-NMR spectra of ligand [$H_2$aeae-sal] (**I**) and [$H_2$aeae-hyap] (**II**) are presented in figure 5 and spectral data are summarized in Table S3. Ligand [$H_2$aeae-sal] (**I**) displays the characteristic (—H-C=N) proton singlet signal at 8.33 ppm along with the four aromatic proton signals in the range of 6.83–7.30 ppm and eight aliphatic proton signals within their expected range (2.74–3.68 ppm). Ligand [$H_2$aeae-hyap] (**II**) shows its characteristic sharp singlet signal at 2.38 ppm due to the –$CH_3$ protons and signals for four aromatic protons are present in the range of 6.71–7.54 ppm. Eight aliphatic proton signals arise within the expected range of 2.75–3.70 ppm. Both ligands are unable to produce any detectable –NH proton signal, although ligand (**II**) displays one broad signal at 16.44 ppm due to the –OH proton.[35] Thus, $^1$H-NMR spectral data strongly supports the structure of ligand (**I**) and (**II**) as suggested in scheme 1.

$^{13}$C NMR spectroscopy was used to confirm the molecular structure of ligand [$H_2$aeae-sal] (**I**) and [$H_2$aeae-hyap] (**II**). $^{13}$C NMR spectra of (**I**) and (**II**) were recorded in DMSO-$d_6$ and shown in Figure 6. As

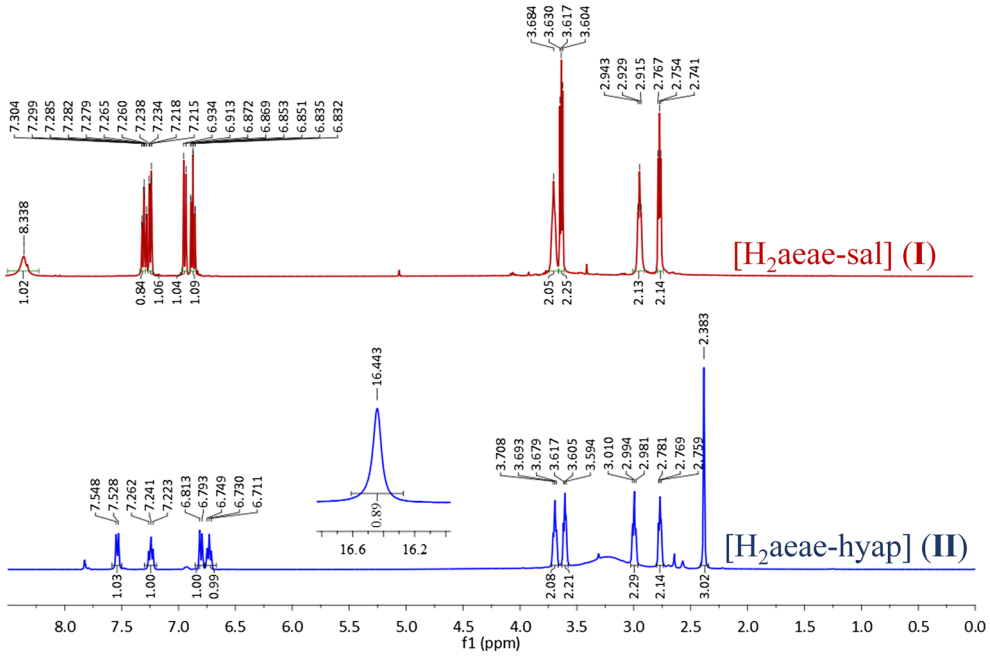


**FIGURE 5** $^{1}$H NMR spectra of [$H_2$aeae-sal] (**I**) and [$H_2$aeae-hyap] (**II**) recorded in $CDCl_3$

expected, ligand (**I**) shows eleven distinctive signals in its $^{13}$C NMR spectrum. The most downfield signal at 166.52 ppm appears due to the azomethine carbon (C7). The signal at 161.09 ppm is due to the phenolic carbon (C1). The rest of the aromatic carbons are present in the range of 116.76–132.27 ppm. There are four signals present in the aliphatic region, out of which the two most downfield signals at 58.57 and 60.42 ppm are due to C11 and C8, respectively, as they are bonded to the electronegative atoms O and N, whereas the other two aliphatic signals appearing at 49.84 and 51.78 ppm are due to C9 and C10, respectively. Ligand (**II**) exhibits a similar type of spectra with one additional signal at 14.52 ppm due to the methyl carbon (C8). As mentioned for ligand **(I)**, here also the azomethine carbon (C7) shows the most downfield signal at 173.22 ppm and the phenolic carbon (C1) at 165.35 ppm. All the other aromatic protons appear in their expected range (116.33–132.86 ppm). Signals due to the rest four aliphatic carbons appear at 48.67 (C10), 49.46 (C11), 51.71 (C9), and 60.57 (C7) ppm. Observed signals and their assignments are tabulated in Table S4 which are in good agreement with the molecular structure proposed by FT-IR and $^{1}$H NMR analyses.

Both vanadium(V) oxido complexes **3** and **4** were characterized in solution through $^{51}$V NMR spectroscopy. The $^{51}$V NMR spectra of complexes [{$V^{V}$O(Haeae-sal)}μ-

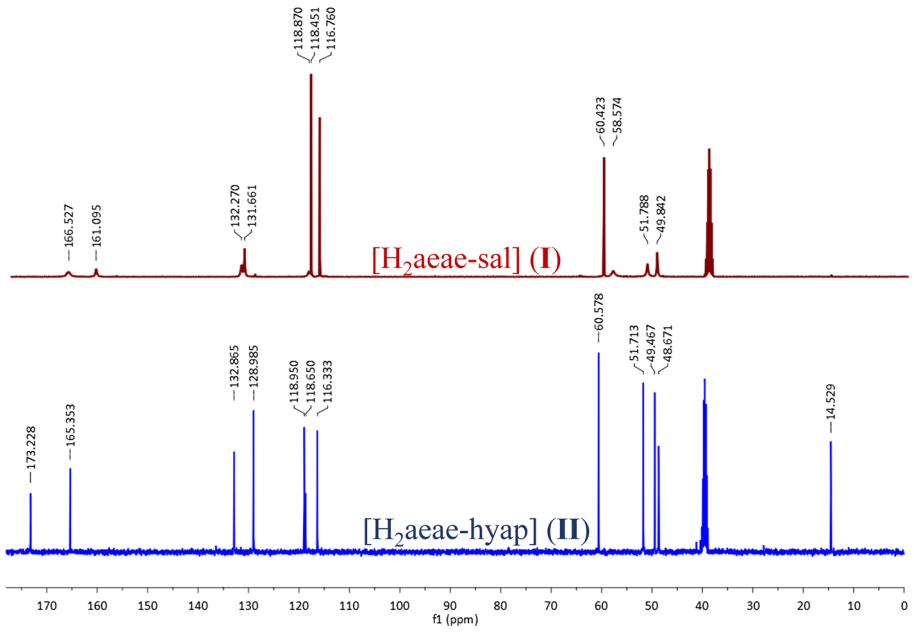


**FIGURE 6** $^{13}$C NMR spectra of [$H_2$aeae-sal] (**I**) and [$H_2$aeae-hyap] (**II**) recorded in DMSO-$d_6$

O]$_2$ (**3**) and [{V$^V$O(Haeae-hyap)}μ-O]$_2$ (**4**) were recorded with a freshly prepared solution in DMSO-$d_6$ while $VOCl_3$ was used as an external reference (shown in Figure 7). Due to the quadrupole interaction, $^{51}$V NMR lines appear slightly broad.[36] Vanadium(V) complexes **3** and **4** exhibit one strong resonance at −528.126 ppm and − 531.467 ppm, respectively, which are within the range of reported V$^V$O$_2$ form of complexes.[37] Along with the intense −531.467 ppm signal, complex **4** shows two additional weaker bands at −511.812 ppm and − 488.801 ppm, which may be due to the coordination of DMSO.[36a,38] The $^{51}$V NMR studies further confirm the existence of the monomeric vanadium(V)dioxide species in solution.

## 6.6 | Single crystal X-ray diffraction studies

The molecular structure of **3** and **4** have been confirmed by single-crystal X-ray analysis. ORTEP diagrams of **3** and **4** are shown in Figure 8 and Figure S6, respectively. Both complexes **3** and **4** crystallizes in the centrosymmetric monoclinic crystal system with space group $P2_1/c$. The asymmetric unit of compounds **3** and **4** carry one half of the dinuclear complex. X-ray analysis shows that both vanadium centers in dinuclear complexes **3** and **4** acquire distorted octahedral geometry while keeping the V1-V1′ distance 3.102 Å and 3.134 Å, respectively. However, each vanadium center in the asymmetric unit adopts a square pyramidal geometry. The basal plane is occupied by one O atom from phenolate moiety, one N atom from azomethine, one N from the amine and one oxido O atom. Another oxido O atom occupies the apical position. One oxido O-atom from each vanadium center

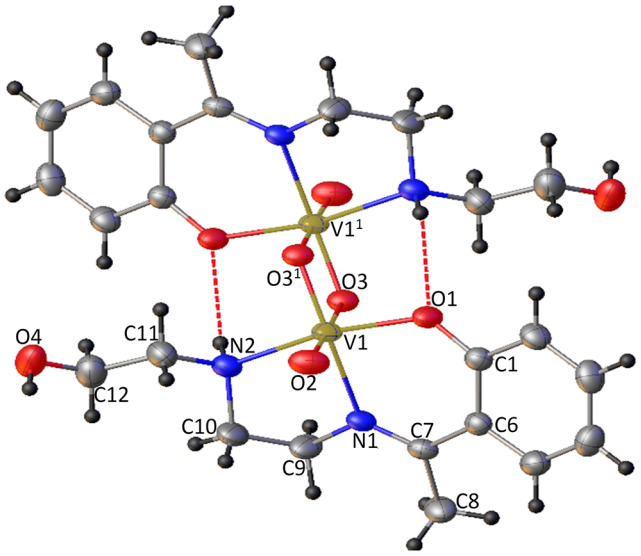


**FIGURE 8** ORTEP diagram of complex [{V$^V$O(Haeae-1 hyap)}-O]$_2$ (4)

coordinates to another vanadium center in the solid-state acting as a bridging ligand and hence produces a dimer. The mutual distance between the two bridging O atoms is 2.566 Å in **3** and 2.596 Å in **4**. The V=O bond distance is 1.612 Å in **3** and 1.609 Å in **4,** which is a characteristic of a strong vanadium oxido (V=O) bond. While much longer V1-O3 bond [1.685 Å in **3** and 1.684 Å in **4**] in the equatorial plane allows O atom to act as a bridging ligand.

A partial list of all the vital bond angles and bond lengths of the complexes **3** and **4** are enlisted in Table S5.

Both intra-molecular and inter-molecular H-bonding is present in complexes **3** and **4**. In complex **3**, a strong intramolecular hydrogen bond (1.941 Å) exists between OH-group of the Schiff-base ligand and one of the

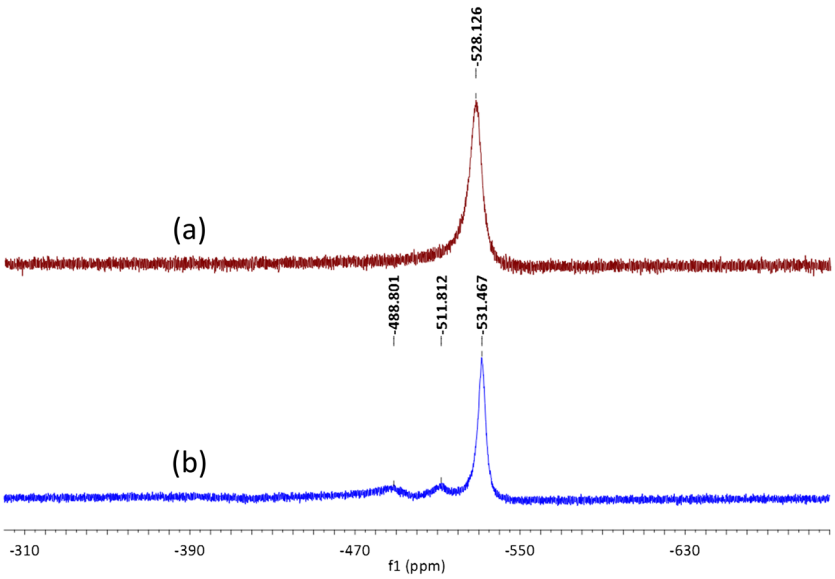


**FIGURE 7** $^{51}$V-NMR spectra of (**A**) [{V$^V$O(Haeae-sal)}μ-O]$_2$ (**3**) and (B) [{V$^V$O(Haeae-hyap)}μ-O]$_2$ (**4**) recorded in DMSO-$d_6$. Chemical shifts (δ) of $^{51}$V are referenced with respected to $VOCl_3$ as an external standard

bridging O-atom (O4-H4⋯⋯ O3). Whereas in **4**, a relatively weak H-bond (2.264 Å) is observed between phenolate O-atom of the Schiff-base ligand and amine H (–NH) atom of the other half of the dimer (O1⋯⋯ H2′-N2′). Stronger H-bonding can be a reason for the shorter V-V′ atom distance in **3** as compared to **4**. Inter-molecular H-bonding in both complexes leads to the molecular association to form a 3D structure in solid state. Detailed H-bonding distances and bond angles are listed in table S6.

## 7 | THEORETICAL STUDIES

### 7.1 | Geometry optimization

Molecular structure of the dimeric vanadium complexes $[\{V^{V}O(aeae\text{-}sal)\}\mu\text{-}O]_2$ (**3**), $[\{V^{V}O(aeae\text{-}hyap)\}\mu\text{-}O]_2$ (**4**) and corresponding monomeric complexes $[V^{V}O_2(aeae\text{-}sal)]$ **3(a)**, $[V^{V}O_2(aeae\text{-}hyap)]$ **4(a)** (shown in the Figure S7), were optimized by using a mixed basis set, DFT/UB3LYP employing LANL2DZ with an effective core potential for V atom and 6-31G (d,p) for the rest of the atoms. Single-crystal XRD structures were used as an initial guess. All the optimized geometrical parameters are listed in Table S5 and shown in Figure S8–S11. There is an excellent agreement between the solid-state data of the single crystals and theoretically calculated data of gas-phase as well as solution phase of the complexes. A slight deviation of the structural parameters can be explained by the approximate basis set chosen for the gas phase and solution phase DFT calculation without considering lattice interactions. The absence of imaginary frequencies indicates the local minima on the potential energy surface. Based on these optimized structures calculations of the other parameters such as polarizability, vibrational frequencies, Natural Bond Orbital (NBO) analysis, etc. were carried out.

With the help of Koopman's theorem[39] electronegativity and chemical hardness of the molecule were calculated. Electrophilicity index (ψ) and global softness were also calculated as calculated by Parr et al.[40] All the above-mentioned quantum chemical properties of monomeric and dimeric vanadium complexes calculated by using UB3LYP/LANL2DZ*U*6-31G (d, p) method are shown in Table 3.

As suggested by single-crystal X-ray analysis, both **3** and **4** can dissociate into corresponding monomeric species in solution due to their elongated V-O bridging distance. So, the theoretical UV–Vis absorption spectra of both the complexes **3** and **4** were determined in their dimeric and monomeric form. TD-DFT calculation was performed on the optimized geometry employing a mixed basis set B3LYP using LANL2DZ with an effective core potential for V atom and 6-31G++(d, p) for the rest of the atoms. All the calculations were performed in methanol using CPCM solvation model. The experimental UV–Vis spectra of the complexes **3** and **4** recorded in methanol were plotted against the theoretically predicted UV–Vis spectra of **3** and **4** in its dimeric as well as monomeric form (shown in Figure 9).

Also selected theoretical absorption spectral maxima (nm), along with their excitation energy (eV) and oscillator strength parameter (*f*) are listed in Table S7. Experimental UV–Vis absorption spectra of **3** and **4** recorded in methanol bear a close resemblance with the theoretically predicted absorption maxima of the respective monomeric unit (shown in Figure 9). Therefore, **3** and **4** exist in its monomeric form in solution which can be further confirmed by the FT-IR analysis of polymer-supported complexes **5** and **6**. Heterogenization was done by dissolving the complexes **3** and **4** in DMF which allows easy dissociation of the dimer into monomer and as a result monomeric units get attached to the polymeric chain. Hence both supported complexes **5** and **6** carry

**TABLE 3** Quantum chemical properties calculated by using DFT/UB3LYP methods with mixed basis set LANL2DZU6-31G(d, p)

| | | Complexes | | | |
|---|---|---|---|---|---|
| **SL.No.** | **Parameters** | **3** | **4** | **$[V^{V}O_2(aeae\text{-}sal)]$ 3(a)** | **$[V^{V}O_2(aeae\text{-}hyap)]$ 4(a)** |
| 1 | HOMO (eV) | −0.2172 | −0.2029 | −0.1329 | −0.2123 |
| 2 | HOMO-1 (eV) | −0.2191 | −0.2042 | −0.2488 | −0.2377 |
| 3 | LUMO (eV) | −0.0700 | −0.0491 | −0.0523 | −0.0671 |
| 4 | LUMO+1 (eV) | −0.0651 | −0.0459 | −0.0434 | −0.0424 |
| 5 | \|ΔE\|(energy gap) (eV) | −0.1472 | −0.1538 | −0.0806 | −0.1452 |
| 6 | χ (eV) (Electronegativity) | 0.1436 | 0.126 | 0.0926 | 0.1397 |
| 7 | η (eV) (Chemical hardness) | −0.0736 | −0.0769 | −0.0403 | −0.0726 |
| 8 | ζ (eV) (softness) | −6.7934 | −6.5019 | −12.4069 | −6.8870 |
| 9 | ψ (eV) (electrophilicity index) | −0.1400 | −0.1032 | −0.1064 | −0.1344 |

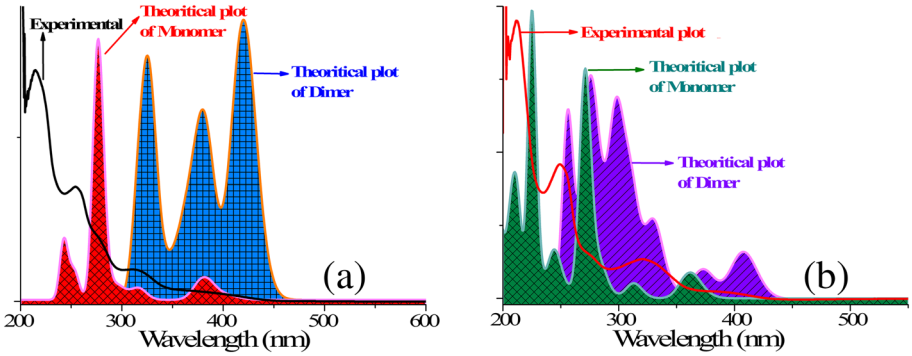


**FIGURE 9** Comparison between experimental and theoretical UV–Vis plots of (A) [{$V^{V}O$(Haeae-sal)}μ-O]$_2$ (**3**) and (B) [{$V^{V}O$(Haeae-hyapl)}μ-O]$_2$ (**4**)

characteristic FT-IR stretching vibration of five coordinated cis-$VO_2$ species in the solid-state.

## 7.2 | TGA and AAS analysis

Thermal stability of the supported complexes PS-[$V^{V}O_2$(Haeae-sal)] (**5**) and PS-[$V^{V}O_2$(Haeae-hyap)] (**6**) was tested by TGA under nitrogen atmosphere at a temperature rate of 10 °C/min over a temperature range of 30 °C to 850 °C (shown in Figure 10). Both complexes **5** and **6** show three-stage thermal decomposition profiles in their TGA curve which is a typical TGA pattern for polymer-supported metal complexes.[35,41] Initially, both complexes **5** and **6** undergo a small mass loss of 3.12% and 6.53%, respectively, due to the loss of physically adsorbed gases and moisture. In the next step, 7.51% (in **5**) and 14.01% (in **6**) of weight loss was observed within the temperature range of 191 °C to 341 °C due to the loss of entrapped solvent (DMF) and water molecules.

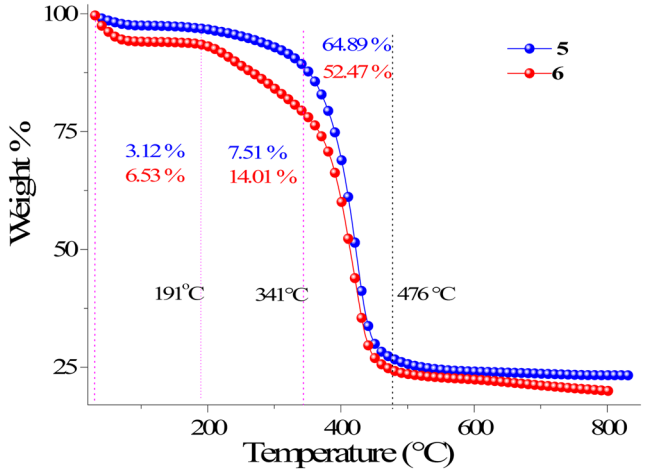


**FIGURE 10** DTA-TGA plots of polymer anchored vanadium complexes **5** and **6**

In the final step, both complexes exhibit a massive mass loss in the temperature range of 341 °C to 476 °C because of the simultaneous breakdown and decomposition of polymer structure as well as metal complexes. Complex **5** shows a mass loss of 64.89% while 52.47% weight loss is observed in **6**. TGA analysis suggests that both supported complexes **5** and **6** are stable up to 341 °C.

## 7.3 | SEM–EDX and AAS analysis

Change in surface morphology during the heterogenization of [{$VO^{V}$(Haeae-sal)}μ-O]$_2$ (**3**) and [{$VO^{V}$(Haeae-hyap)}μ-O]$_2$ (**4**) into the polymeric chain was analyzed by SEM. The change in elemental composition was examined by the energy-dispersive X-ray (EDX) analysis. SEM and elemental mapping of PS-[$V^{V}O_2$(Haeae-sal)] (**5**) and PS-[$V^{V}O_2$(Haeae-hyap)] (**6**) was done and shown in Figure 11 and S12.

As expected, pure chloromethylated polystyrene bead shows flat and smooth surface containing only the signals of carbon, hydrogen and chlorine atoms (Figure S13, the SEM and EDX image of pure polymer bead is reproduced from our earlier paper).34c Both polymer-supported complexes show the elemental signal of oxygen and nitrogen along with the signal of vanadium atoms in their elemental mapping images. A semi-quantitative measurement, EDX, indicates 5.4% and 5.5% of vanadium content in complex **5** and **6,** respectively. All this information suggests successful covalent attachment of complexes **3** and **4** into the chloromethylated polystyrene bead. Exact vanadium loading into the polymer support was estimated by atomic absorption spectroscopy, which is found to be 0.44625% (0.0876 mmol/g) and 1.043% (0.20474 mmol/g) in complex **5** and **6**, respectively (Table S8). Elemental maps of important atoms along with the SEM images of the recycled catalysts **5** and **6** were also analyzed. Similar SEM images to that of fresh catalysts indicate no change in morphology as well as the

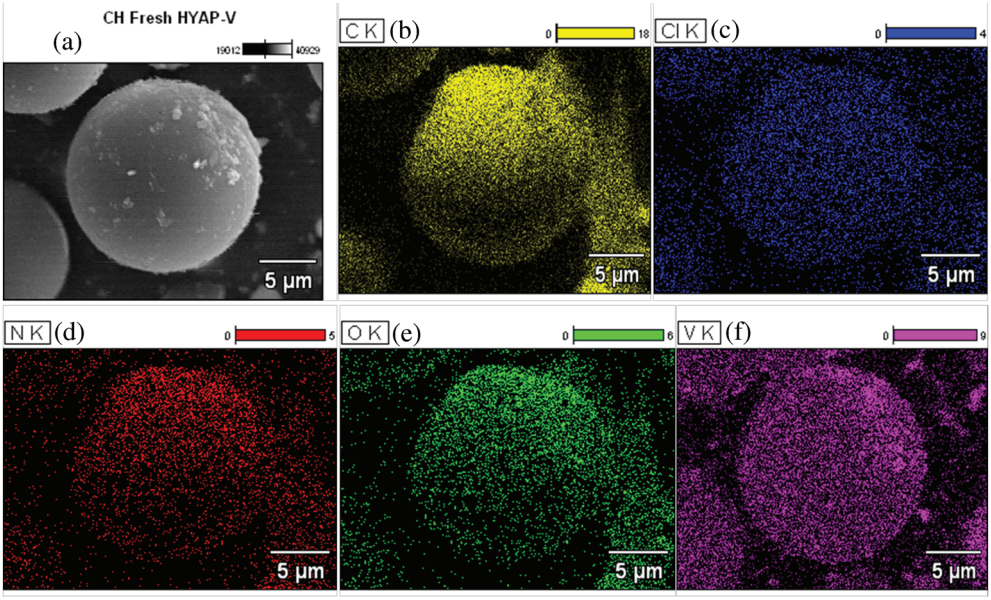


**FIGURE 11** (A) SEM image of single polymer bead of catalyst PS-[$V^{V}O_2$(Haeae-hyap)] (**6**) and corresponding elemental mapping of (B) carbon, (C) chlorine, (D) nitrogen, (E) oxygen, and (F) vanadium with EDX

physical form of the catalysts even after multiple uses in a catalytic reaction. However, vanadium mapping of the used catalysts shows slightly less density of vanadium atoms (Figure S14 and S15) in comparison to the neat one. This is due to the removal of excess adsorbed metal complexes from the upper surface of the polymer bead along with a small amount of metal leaching from the polymer matrix during the catalytic reaction.

## 7.4 | AFM analysis

Although the SEM images are quite informative regarding the change in surface morphology during heterogenization, atomic force microscopy provides a quantitative idea regarding changes in surface roughness during the heterogenization process. The average surface roughness of pure polymer bead along with supported complexes and their corresponding recycled supported complexes was analyzed by AFM and shown in Figure 12 and Figure S16 (Figure 12(A), AMF image of pure polymer bead is reproduced from our earlier paper).[42] The surface roughness and mean height of polymer resin (PS-Cl) are 10.1 nm and 78.0 nm, respectively. AFM image clearly shows that after covalent attachment of **3** and **4** into the polymeric chain of chloromethylated polystyrene surface roughness and mean height reduces. The average surface roughness of complex **5** and **6** is 3.21 nm and 2.88 nm, respectively. Due to the anchoring of metal complexes into the pores of the polymer chain during heterogenization causes the reduction in surface roughness.[42–46] Hence, surface roughness can be

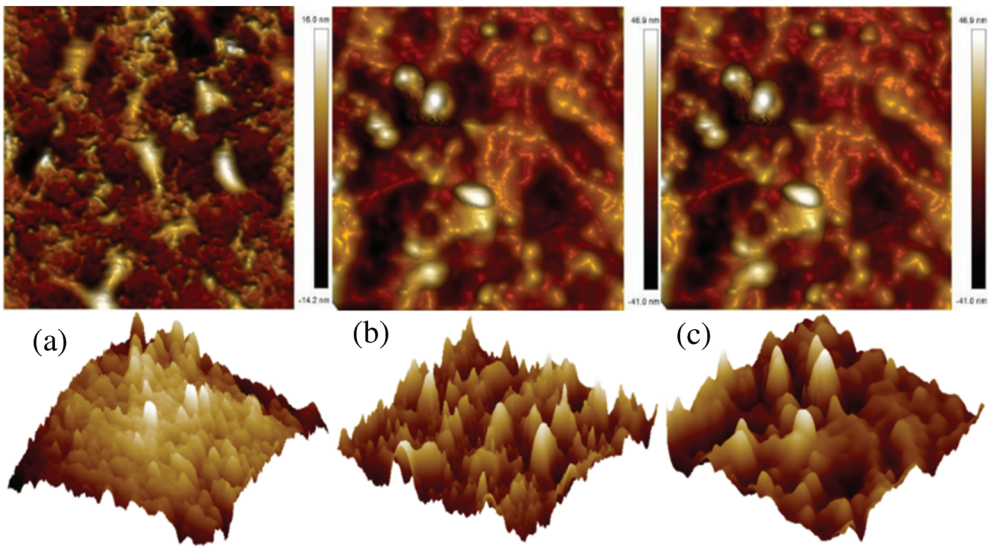


**FIGURE 12** AFM pictures and corresponding 3D-surface maps of (A) PS-Cl, (B) PS-[$V^{V}O_2$(Haeae-sal)] (**5**) (C) PS-[$V^{V}O_2$(Haeae-hyap)] (**6**)

correlated with the percentage of metal loading into the polymer. The lower average surface roughness of complex **6** than **5** indicates a higher percentage of metal loading in complex **6** in comparison to complex **5**. AAS analysis data of complexes **5** and **6** also supports the above facts. Detailed surface roughness along with the Root Mean Square (RMS) roughness (Rq) and mean height of both complexes **5** and **6** are listed in Table S9. As mentioned in EDX analysis, the surface roughness of the recycled complexes increases (shown in the Figure S15) to some extent due to the removal of excess adsorbed metal complexes from the upper surface of the polymer bead along with a small amount of metal leaching during the catalytic reaction. The estimated average surface roughness of the recycled catalysts **5** and **6** are 4.27 nm and 3.11 nm, respectively.

## 8 | CATALYTIC ACTIVITY STUDIES

### 8.1 | Oxidative bromination of Salicylaldehyde

Vanadium haloperoxidase, a vanadium-containing metalloenzyme, selectively catalyzes the oxidation of halide in the presence of hydrogen peroxide, and, if any suitable organic substrate is available, then it can halogenate the organic substrate also.[47–49]

The catalytic activity of PS-[$V^VO_2$(Haeae-sal)] (**5**) and PS-[$V^VO_2$(Haeae-hyap)] (**6**) was studied for the oxidative bromination of salicylaldehyde. It is observed that the vanadium complexes **5** and **6** successfully catalyze the oxidative bromination of salicylaldehyde in the presence of hydrogen peroxide and hence become the functional models of vanadium bromoperoxidase. Three major oxidative bromination products i.e. 5-bromo-2-hydroxyl benzaldehyde (5-BrS), 3-bromo-2-hydroxy benzaldehyde (3-BrS) and 3, 5-dibromo-2-hydroxybenzaldehyde (3,5-BrS), were identified during the catalytic reaction (Scheme 2).[35,50–56] PS-[$V^VO_2$(Haeae-sal)] (**5**) was used as a representative catalyst during the optimization of different reaction parameters namely amount of catalyst, amount of oxidant (30% aqueous $H_2O_2$), amount of perchloric acid, amount of potassium bromide and amount of solvent, while keeping other reaction conditions such as RPM of magnetic stirrer, size of magnetic bead, shape and size of reaction flask, etc. as identical as possible (Figure 13). In the oxidative bromination, half of the perchloric acid was added at the beginning of the reaction ($t$ = 0 min), and the rest of the amount was added to the reaction mixture in three equal portions at a fixed time interval (after every 15 min). In all cases prior

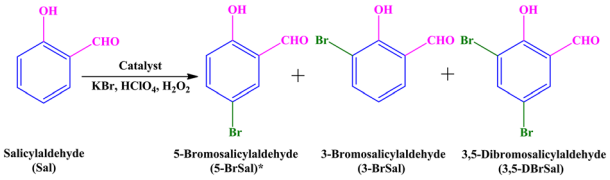


**SCHEME 2** Oxidative bromination products of salicylaldehyde [(*) major product)]

to the reaction, polymer anchored catalysts were swelled in water for 12 hr.

Detailed results of all the reaction conditions applied to optimize oxidative bromination of salicylaldehyde in the presence of catalyst **5** are summarized in Table 4. Entry No. 17 of Table 4 represents the optimized reaction conditions for the oxidative bromination of salicylaldehyde which are, 10 mmol of salicylaldehyde (1.22 g), catalyst 0.005 g, 15 mmol of $H_2O_2$ (1.7025 g), 20 mmol of KBr (2.38 g), 20 mmol of $HClO_4$ (2.86 g), 15 ml water, 2 hr of time and room temperature.

A blank reaction under the same optimized reaction conditions shows only 47.7% substrate conversion. Neat complexes (**3** and **4**) were also employed as catalysts for the oxidative bromination of salicylaldehyde under optimized reaction conditions. Catalyst **3** and **4** show 94.4% and 79.0% conversions, respectively. Both supported and neat catalysts produce 5-BrS as the major product. However, the decrease in product selectivity (%), as well as substrate conversion (%), was observed while using neat catalysts. Surprisingly, catalysts **3–6** show exceptionally high TOF values during the catalytic oxidative bromination of salicylaldehyde.[50,52,53,55–60] The TOF values of the neat complexes are quite low in comparison to that of grafted catalysts (See Table 4). Therefore heterogenization of the homogeneous catalysts **3** and **4** not only preserve the catalytic efficiency but also improves the effectiveness significantly. Considering the TOF values, catalyst **5** is more efficient (TOF = $1.127 \times 10^4$ $h^{-1}$) in comparison to the catalyst **6** ($4.675 \times 10^3$ $h^{-1}$). Detailed comparison of catalytic efficiency of the supported catalysts **5** and **6,** along with their corresponding neat counterparts **3** and **4,** for the oxidative bromination of salicylaldehyde is presented in Figure 14. So far several vanadium complexes are known to catalyze the oxidative bromination of salicylaldehyde in the presence of $H_2O_2$ but none of them does the job as efficiently as polymer-supported complexes **5** and **6**.13b, 33

### 8.2 | Oxidation of thioanisole

Besides catalyzing the oxidation of halides in the presence of hydrogen peroxide, vanadium haloperoxidase can

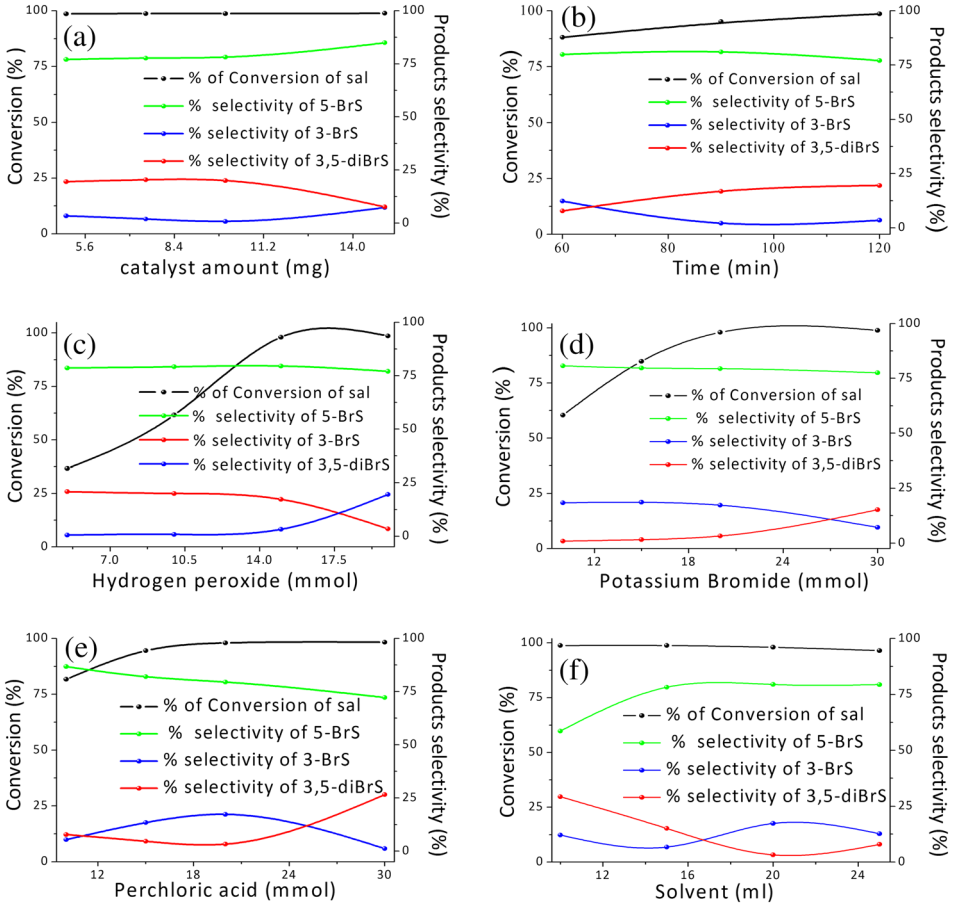


**FIGURE 13** Catalytic oxidative bromination of salicylaldehyde by hydrogen peroxide in the presence of **5** at room temperature (A) Impact of amount of catalyst, (B) Effect of time, (C) Effect of oxidant ($H_2O_2$) amount, (D) Impact of KBr amount and (E) Effect of $HClO_4$ amount and (F) influence of solvent amount

also accelerate the oxidation and oxo transfer reaction in aromatic compounds, including the oxidation of thioether into sulfone and sulfoxide. Oxidative desulfurization of organic sulfides is an important reaction in the drug and petroleum industry.11b, 61–63 Therefore, the catalytic efficiency of synthesized catalysts, PS-[$V^VO_2$(Haeae-sal)] (**5**) and PS-[$V^VO_2$(Haeae-hyap)] (**6**), was evaluated for the oxidation of thioanisole. Sulfone and sulfoxide were identified as two major products (shown in scheme 3) for this reaction which are well reported in the literature.[43,61,64–68]

In order to attain the maximum substrate conversion(%), various reaction conditions such as reaction time, amount of catalyst, amount of oxidant ($H_2O_2$), the volume of solvent (acetonitrile) and nature of solvent were optimized, while using PS-[$V^VO_2$(Haeae-hyap)] (**6**) as a representative catalyst (Shown in Figure S17).

All the results of various reaction conditions to identify the optimized reaction parameters of oxidation of thioanisole catalyzed by catalyst **6** are listed in Table 5. Data in Table 5 conclude that 1.417 g (12.5 mmol) of 30% $H_2O_2$ was required to achieve maximum conversion (%) during the oxidation of thioanisole (5 mmol, 0.627 g) in the presence of 0.020 g catalyst **6** and 4 ml of ethanol at room temperature for 4 hr of reaction time. Under the above-optimized reaction conditions oxidation of thioanisole was performed in four different solvents like EtOH, ACN, DMF, and hexane. A maximum of 90.7% conversion was observed in ethanol whereas acetonitrile, DMF and hexane showed 85.5%, 78.6%, and 72.3% conversion, respectively (shown in Figure S17(E)). These results indicate that substrate conversion (%) increases with the increase of polarity of solvents. So, EtOH was chosen as the reaction solvent. Neat catalysts [{$V^VO$(aeae-sal)}μ-O]$_2$ (**3**), [{$V^VO$(Haeae-hyap)}μ-O]$_2$ (**4**) and supported catalyst PS-[$V^VO_2$(Haeae-sal)] (**5**) show 75.2%, 84.5%, and 80.1% conversion respectively under the above mentioned optimized reaction conditions. The controlled reaction shows only 32.5% conversion.

Detailed comparison of oxidation of thioanisole by the grafted catalysts **5**, **6** and neat complexes **3, 4** is presented in Figure 15. Data in Table 5 shows that homogeneous oxidative desulfurization by catalysts **3** and **4** is a little less effective in terms of substrate conversion (%), product selectivity (%) or TOF values when compared to their heterogeneous counterparts **5** and **6**. Both homogeneous and heterogeneous catalytic oxidative desulfurization produces sulfoxide as the major product unanimously.

**TABLE 4** Summarized results of all the reaction conditions applied to optimize the maximum oxidative bromination of salicylaldehyde by catalyst **5** at room temperature

| SN | Cat. | Cat. (mg) | Sub: Oxn | $HClO_4$ (mmol) | Time (min) | KBr (mmol) | Solvent (ml) | % Conversion | TOF/h | % Selectivity (%) 5-BrS | (%) 3-BrS | (%) 3,5-di-BrS |
|---|---|---|---|---|---|---|---|---|---|---|---|---|
| 1 | 5 | 7.5 | 1:2 | 20 | 120 | 20 | 20 | 98.7 | $7.511 \times 10^3$ | 77.64 | 1.94 | 20.41 |
| 2 | 5 | 10 | 1:2 | 20 | 120 | 20 | 20 | 98.7 | $5.633 \times 10^3$ | 78.15 | 0.81 | 21.03 |
| 3 | 5 | 15 | 1:2 | 20 | 120 | 20 | 20 | 98.8 | $3.759 \times 10^3$ | 84.92 | 7.4 | 7.67 |
| 4 | 5 | 5 | 1:2 | 20 | 60 | 20 | 20 | 88.1 | $2.011 \times 10^4$ | 79.66 | 12.30 | 7.75 |
| 5 | 5 | 5 | 1:2 | 20 | 90 | 20 | 20 | 95.1 | $1.447 \times 10^4$ | 80.40 | 2.24 | 16.82 |
| 6 | 5 | 5 | 1:2 | 20 | 120 | 20 | 20 | 98.6 | $1.125 \times 10^4$ | 77.02 | 3.46 | 19.52 |
| 7 | 5 | 5 | 2:1 | 20 | 120 | 20 | 20 | 36.6 | $4.178 \times 10^3$ | 78.6 | 20.85 | 0.54 |
| 8 | 5 | 5 | 1:1 | 20 | 120 | 20 | 20 | 61.6 | $7.031 \times 10^3$ | 79.11 | 20.02 | 0.86 |
| 9 | 5 | 5 | 2:3 | 20 | 120 | 20 | 20 | 98.0 | $1.118 \times 10^4$ | 79.47 | 17.28 | 3.24 |
| 10 | 5 | 5 | 2:3 | 20 | 120 | 10 | 20 | 60.4 | $6.894 \times 10^3$ | 80.7 | 18.4 | 0.89 |
| 11 | 5 | 5 | 2:3 | 20 | 120 | 15 | 20 | 84.9 | $9.691 \times 10^3$ | 79.75 | 18.64 | 1.6 |
| 12 | 5 | 5 | 2:3 | 20 | 120 | 30 | 20 | 98.9 | $1.128 \times 10^4$ | 77.56 | 7.19 | 15.24 |
| 13 | 5 | 5 | 2:3 | 10 | 120 | 20 | 20 | 81.7 | $9.326 \times 10^3$ | 86.8 | 5.38 | 7.81 |
| 14 | 5 | 5 | 2:3 | 15 | 120 | 20 | 20 | 94.5 | $1.078 \times 10^4$ | 81.99 | 13.37 | 4.63 |
| 15 | 5 | 5 | 2:3 | 30 | 120 | 20 | 20 | 98.3 | $1.122 \times 10^4$ | 72.23 | 1.2 | 26.56 |
| 16 | 5 | 5 | 2:3 | 20 | 120 | 20 | 10 | 98.8 | $1.127 \times 10^4$ | 58.63 | 12.10 | 29.25 |
| 17 | 5 | 5 | 2:3 | 20 | 120 | 20 | 15 | 98.8 | $1.127 \times 10^4$ | 78.24 | 6.72 | 15.03 |
| 18 | 5 | 5 | 2:3 | 20 | 120 | 20 | 25 | 96.5 | $1.101 \times 10^4$ | 79.42 | 12.67 | 7.9 |
| 19 | 3 | 5 | 2:3 | 20 | 120 | 20 | 15 | 94.4 | $2.739 \times 10^2$ | 62.09 | 26.80 | 5.52 |
| 20 | 4 | 5 | 2:3 | 20 | 120 | 20 | 15 | 79.0 | $2.403 \times 10^2$ | 55.82 | 22.08 | 1.17 |
| 21 | 6 | 5 | 2:3 | 20 | 120 | 20 | 15 | 95.7 | $4.675 \times 10^3$ | 75.16 | 15.75 | 4.24 |
| 22 | - | 5 | 2:3 | 20 | 120 | 20 | 15 | 47.7 | - | 37.91 | 8.95 | 0.91 |

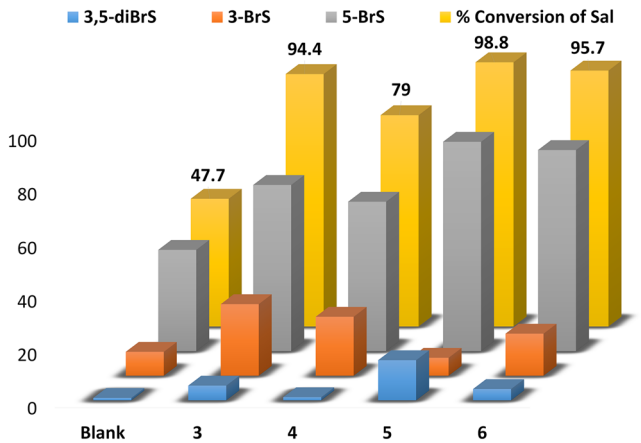


**FIGURE 14** Comparative plot of % conversion of salicylaldehyde by using catalysts **3**, **4**, **5** and **6** with blank reaction

## 8.3 | Recyclability test

After their use in completion of one catalytic cycle, polymer anchored metal complexes **5** and **6** were filtered off and washed with DMF followed by methanol, and dried in an oven under 120 °C for 24 hr. Recycled catalysts were used multiple times in the catalytic oxidative bromination of salicylaldehyde and oxidation of thioanisole

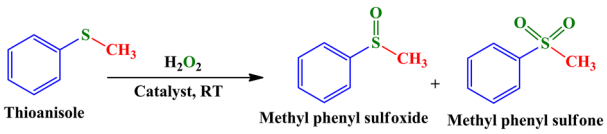


**SCHEME 3** Oxidation of thioanisole by the catalysts in the presence of oxidant $H_2O_2$

**TABLE 5** Results of oxidation of Thioanisole catalyzed by catalyst **6**. Conversion (%) and selectivity (%) of products obtained at different parameters in 4 hr at room temperature

| S. N. | Cat. | Cat. (mg) | Substrate: Oxidant | Solvent (ml) | Solvent | Time (hr.) | % Conv. | TOF/h | % Selectivity | |
|---|---|---|---|---|---|---|---|---|---|---|
| | | | | | | | | | Sulfoxide | Sulfone |
| 1 | 6 | 20 | 1:2 | 10 | ACN | 1 | 44.4 | $5.422 \times 10^2$ | 56.88 | 43.11 |
| 2 | 6 | 20 | 1:2 | 10 | ACN | 2 | 58.0 | $3.541 \times 10^2$ | 54.01 | 45.98 |
| 3 | 6 | 20 | 1:2 | 10 | ACN | 3 | 64.9 | $2.642 \times 10^2$ | 51.48 | 48.51 |
| 4 | 6 | 20 | 1:2 | 10 | ACN | 5 | 69.2 | $1.690 \times 10^2$ | 63.06 | 36.93 |
| 5 | 6 | 10 | 1:2 | 10 | ACN | 4 | 49.9 | $3.047 \times 10^2$ | 58.88 | 41.11 |
| 6 | 6 | 15 | 1:2 | 10 | ACN | 4 | 55.7 | $2.267 \times 10^2$ | 65.31 | 34.68 |
| 7 | 6 | 20 | 1:2 | 10 | ACN | 4 | 68.9 | $2.103 \times 10^2$ | 67.42 | 32.57 |
| 8 | 6 | 25 | 1:2 | 10 | ACN | 4 | 68.5 | $1.673 \times 10^2$ | 67.79 | 32.21 |
| 9 | 6 | 30 | 1:2 | 10 | ACN | 4 | 67.4 | $1.371 \times 10^2$ | 65.48 | 34.51 |
| 10 | 6 | 20 | 1:1 | 10 | ACN | 4 | 20.0 | $6.106 \times 10^1$ | 79.44 | 20.55 |
| 11 | 6 | 20 | 2:3 | 10 | ACN | 4 | 38.2 | $1.166 \times 10^2$ | 73.94 | 26.05 |
| 12 | 6 | 20 | 2:5 | 10 | ACN | 4 | 85.3 | $2.604 \times 10^2$ | 64.37 | 35.62 |
| 13 | 6 | 20 | 2:5 | 4 | ACN | 4 | 85.5 | $2.610 \times 10^2$ | 64.20 | 35.79 |
| 14 | 6 | 20 | 2:5 | 7 | ACN | 4 | 87.0 | $2.656 \times 10^2$ | 64.42 | 36.54 |
| 15 | 6 | 20 | 2:5 | 13 | ACN | 4 | 87.5 | $2.671 \times 10^2$ | 64.21 | 35.78 |
| 16 | 6 | 20 | 2:5 | 4 | EtOH | 4 | 90.7 | $2.769 \times 10^2$ | 79.58 | 20.41 |
| 17 | 6 | 20 | 2:5 | 4 | DMF | 4 | 78.6 | $2.399 \times 10^2$ | 78.71 | 21.28 |
| 18 | 6 | 20 | 2:5 | 4 | Hexane | 4 | 72.3 | $2.207 \times 10^2$ | 75.10 | 24.89 |
| 19 | 3 | 20 | 2:5 | 4 | EtOH | 4 | 75.2 | $1.363 \times 10^1$ | 74.60 | 25.39 |
| 20 | 4 | 20 | 2:5 | 4 | EtOH | 4 | 84.5 | $1.606 \times 10^2$ | 79.48 | 20.51 |
| 21 | 5 | 20 | 2:5 | 4 | EtOH | 4 | 81.1 | $5.786 \times 10^2$ | 84.55 | 15.44 |
| 22 | - | 20 | 2:5 | 4 | EtOH | 4 | 32.5 | - | 87.59 | 12.4 |

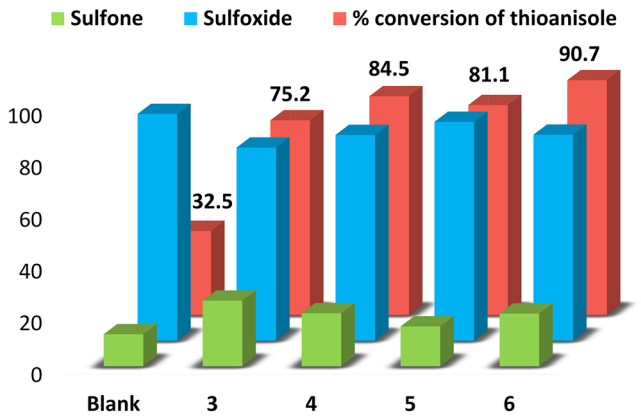


**FIGURE 15** Comparative plot of oxidation of thioanisole under optimized reaction conditions in the presence of catalysts **3**, **4**, **5** and **6** along with blank reaction

under optimized reaction conditions, and the related data is presented in Figure S18. Observed substrate conversion (%) in the presence of recycled catalysts is well within the range of experimental errors that support their heterogeneous nature. Recycled catalysts are also characterized extensively through various techniques like FT-IR, UV–Vis, SEM, EDX, etc. Figure 3 and Figure S5 present the FT-IR spectra of recycled catalysts. All the important characteristic stretching vibrations are preserved in the FT-IR spectra of the recycled catalysts suggesting the existence of catalysts inside the polymer chain. Comparable UV–Vis spectral pattern of the recycled catalysts to that of fresh catalysts (shown in Figure S2) supports the FT-IR analysis. Unchanged physical form and surface morphology were seen in the SEM images (shown in Figure S14 and S15) of the recycled catalysts even after two cycles of catalysis. Vanadium mapping (shown in Figure S14 and S15) on the surface of recycled catalysts confirms the presence of vanadium complexes in the chloromethylated polystyrene beads. Although, the observed vanadium atom density is slightly less in recycled catalysts in comparison to the fresh catalysts. This is because of the inherent inhomogeneity associated with the process of heterogenization of vanadium complexes with the individual polymer beads as well as

the removal of few surfaces adsorbed metal complexes during the course of the catalytic reaction.

## 9 | CONCLUSIONS

Monomeric vanadium (IV) complexes $[V^{IV}O(aeae\text{-}sal)(MeOH)]^+$ **(1)**, $[V^{IV}O(aeae\text{-}hyap)(MeOH)]^+$ **(2)** and dimeric vanadium(V) dioxido complexes $[\{V^{V}O(aeae\text{-}sal)\}\mu\text{-}O]_2$ (**3**), $[\{V^{V}O(Haeae\text{-}hyap)\}\mu\text{-}O]_2$ (**4**) were synthesized and characterized in details by various characterization techniques. Vanadium (IV) oxido complexes are susceptible to molecular oxygen in solution and can quickly be oxidized into vanadium(V) dioxido complexes. The theoretical study, solution-phase UV–vis spectra and FT-IR spectral study of the supported vanadium complexes prove the monomeric nature of vanadium(V) dioxido complexes in solution. Both the complexes **3** and **4** isolated as a dimer in solid-state which is supported by Single-crystal XRD analysis. Catalysts **3** and **4** efficiently catalyze the oxidative bromination of salicylaldehyde and oxidation of thioanisole in presence of hydrogen peroxide. Anchoring the complexes **3** and **4** into the polymer chain enhances the catalytic efficiency many folds for both the catalytic reactions. Under optimized reaction conditions for the oxidative bromination of salicylaldehyde, catalyst **5** shows 98.8% substrate conversion with a TOF value of $1.127 \times 10^4\ h^{-1}$ whereas 95.7% conversion was achieved by **6** with a TOF value of $4.675 \times 10^4\ h^{-1}$, which is quite high in terms of available supported vanadium catalyst in the literature. Whereas for the oxidation of thioanisole, catalysts **5** and **6** exhibit 81.1% (TOF $5.786 \times 10^2\ h^{-1}$) and 90.7% (TOF $2.769 \times 10^2\ h^{-1}$) substrate conversion respectively. Both the vanadium(V) dioxido complexes successfully mimic the functional model of vanadium bromoperoxidase. Uncomplicated synthesis, higher stability, using green oxidant, easy separation, recyclability, and very high TOF values make the reported catalysts best among the available polymer-supported vanadium complexes for the oxidative bromination of salicylaldehyde and oxidation of thioanisole.

## ACKNOWLEDGEMENTS

C. H. thanks the Science and Engineering Research Board (SERB), Department of Science and Technology (DST), the Government of India, New Delhi, for financial support (grant no. SB/EMEQ-055/2014) of the work. A. M, N. K. and P. K. are thankful to IIT (ISM) Dhanbad for fellowship. The authors would like to thank Dr. G. C. Nayak Department of Chemistry, IIT (ISM) Dhanbad, India for SEM/EDX analysis. The authors would like to thank SAIF IIT Mumbai for TGA/DTA and EPR analysis. The authors acknowledge CRF IIT (ISM) Dhanbad for providing single-crystal XRD and AFM analysis. Authors are thankful to NMR Research Centre (SIF) Indian Institute of Science Bangalore for $^{51}V$ NMR analysis. The authors would like to thank DST-FIST (project no. SR/FST/CSI-256) for 400 MHz NMR facility in the department of chemistry IIT (ISM) Dhanbad. GC used in this study was procured from the grant given by Science and Engineering Research Board (SERB), Department of Science and Technology (DST), grant no SB/FT/CS-027/2014), Government of India, New Delhi, India, to C. H. Special thanks to Dr. H. P. Nayek, Department of Chemistry for solving the single crystal XRD data.

## CONFLICT OF INTEREST

There are no conflicts of interest to declare.

## ORCID

*Abhishek Maurya* https://orcid.org/0000-0001-6977-9532

*Chanchal Haldar* https://orcid.org/0000-0003-4642-7918

## REFERENCES

[1] (a)C. Leblanc, H. Vilter, J. B. Fournier, L. Delage, P. Potin, E. Rebuffet, G. Michel, P. L. Solari, M. C. Feiters, M. Czjzek, *Coord. Chem. Rev.* **2015**, *301*, 134. (b)H. Y. Zhao, Y. H. Xing, Y. Z. Cao, Z. P. Li, D. M. Wei, X. Q. Zeng, M. F. Ge, *J. Mol. Struct.* **2009**, *938*, 54. (c)C. J. Schneider, J. E. Penner-Hahn, V. L. Pecoraro, *J. Am. Chem. Soc.* **2008**, *130*, 2712. (d) C. Wikete, P. Wu, G. Zampetlla, L. D. Gioia, G. Licini, D. Rehder, *Inorg. Chem.* **2007**, *46*, 196.

[2] C. R. Cornman, E. P. Zovinka, M. H. Meixner, *Inorg. Chem.* **1995**, *34*, 5099.

[3] (a)Y. Tanabe, Y. Nishibayashi, *Coord. Chem. Rev.* **2019**, *381*, 135. (b)T. S. Smith, C. A. Root, J. W. Kampf, P. G. Rasmussen, V. L. Pecoraro, *J. Am. Chem. Soc.* **2000**, *122*, 767.

[4] (a)D. C. Crans, J. J. Smee, E. Gaidamauskas, L. Q. Yang, *Chem. Rev.* **2004**, *104*, 849. (b)J. H. McNeill, V. G. Yuen, H. R. Hoveyda, C. Orvig, *J. Med. Chem.* **1992**, *35*, 1489.

[5] K. H. Thompson, J. H. McNeill, C. Orvig, *Chem. Rev.* **1999**, *99*, 2561.

[6] (a)H. Pellissier, *Coord. Chem. Rev.* **2015**, *284*, 93. (b)V. Conte, A. Coletti, B. Floris, G. Licini, C. Zonta, *Coord. Chem. Rev.* **2011**, *255*, 2165. (c)E. Amadio, R. D. Lorenzo, C. Zonta, G. Licini, *Coord. Chem. Rev.* **2015**, *301*, 147. (d)N. Mizuno, K. Kamata, *Coord. Chem. Rev.* **2011**, *255*, 2358.

[7] D. Rehder, *J. Inorg. Biochem.* **2008**, *102*, 1152.

[8] (a)C. R. Cornman, J. Kampf, M. S. Lah, V. L. Pecoraro, *Inorg. Chem.* **1992**, *31*, 2035A. (b)A. Messerschmidt, L. Prade, R. Wever, *Biol. Chem.* **1997**, *378*, 309.

[9] (a)M. R. Maurya, S. Khurana, W. Zhang, D. Rehder, *Dalton Trans.* **2002**, 3015. (b)D. Rehder, *Coord. Chem. Rev.* **1999**, *182*, 297.

[10] H. Vilter, *Met. Ions Biol. Syst.* **1995**, *31*, 325.

[11] (a)C. Bolm, *Coord. Chem. Rev.* **2003**, *237*, 245. (b)I. Fernandez, N. Khiar, *Chem. Rev.* **2003**, *103*, 3651. (c)T. S. Smith, V. L. Pecoraro, *Inorg. Chem.* **2002**, *41*, 6754. (d)M. Andersson, A. Willetts, S. Allenmark, *J. Org. Chem.* **1997**, *62*, 8455. (e) C. Bolm, F. Bienewald, *Angew. Chem. Int. Ed. Engl.* **1995**, *34*, 2640. (f)A. H. Vetter, A. Berkessel, *Tetrahedron Lett.* **1998**, *39*, 1741. (g)D. A. Cogan, G. Liu, K. Kim, B. J. Ellmon, *J. Am. Chem. Soc.* **1998**, *120*, 8011. (h)W. Adam, D. Golsch, J. Sundermeyer, G. Wahl, *Chem. Ber.* **1996**, *129*, 1177. (i) K. Nakajima, K. Kojima, M. Kojima, J. Fujita, *Bull. Chem. Soc. Jpn.* **1990**, *63*, 2620.

[12] (a)E. Steffensmeier, K. M. Nicholas, *Chem. Commun.* **2018**, *54*, 790. (b)M. K. Renuka, V. Gayathri, *Catal. Lett.* **2019**, *149*, 1266. (c)I. Syiemlieh, M. Asthana, R. A. Lal, *Appl. Organomet. Chem.* **2019**, *33*, 4984. (d)E. Steffensmeier, M. T. Swann, K. M. Nicholas, *Inorg. Chem.* **2019**, *58*, 844. (e)J. Wang, L. M. D. R. S. Martins, A. P. C. Ribeiro, S. A. C. Carabineiro, J. L. Figueiredo, A. J. L. Pombeiro, *Chem. – Asian J.* **2017**, *1915*, 12. (f)H. H. Monfared, V. Abbasi, A. Rezaei, M. Ghorbanloo, A. Aghaei, *Transition Met. Chem.* **2012**, *37*, 85. (g)N. Mizuno, K. Kamata, *Coord. Chem. Rev.* **2011**, *255*, 2358.

[13] (a)I. Saikia, A. J. Borah, P. Phukan, *Chem. Rev.* **2016**, *116*, 6837. (b)F. Sabuzi, G. Pomarico, B. Floris, F. Valentini, P. Galloni, V. Conte, *Coord. Chem. Rev.* **2019**, *385*, 100.

[14] J. Kaspersma, C. Doumena, S. Munrob, A. M. Prinsa, *Polym. Degrad. Stab.* **2002**, *77*, 325.

[15] L. D. Turner, *J. Food Sci.* **1972**, *37*, 791.

[16] (a)M. K. Renner, P. R. Jensen, W. Fenical, *J. Org. Chem.* **1998**, *63*, 8346. (b)C. S. Neumann, D. G. Fujimori, C. T. Walsh, *Chem. Biol.* **2008**, *15*, 88. (c)G. W. Gribble, *Chemosphere* **2003**, *52*, 289.

[17] (a)D. Wischang, O. Breucher, J. Hartung, *Coord. Chem. Rev.* **2011**, *255*, 2204. (b)D. Wischang, J. Hartung, *Tetrahedron* **2011**, *67*, 4048. (c)M. Eissen, D. Lenoir, *Chem. – Eur. J.* **2008**, *14*, 9830.

[18] (a)X. Li, M. S. Lah, V. L. Pecoraro, *Inorg. Chem.* **1988**, *27*, 4657. (b)S. Y. Liu, Y. P. Ma, *Synth. React. Inorg. Met.-Org. Nano-Metal* **2012**, *42*, 603. (c)X. J. Zhao, L. W. Xue, G. Q. Zhao, *Synth. React. Inorg. Met.-Org. Nano-Metal* **2013**, *43*, 1344. (d)M. J. Xie, Y. F. Niu, X. D. Yang, W. P. Liu, L. Li, L. H. Gao, S. P. Yan, Z. H. Meng, *Eur. J. Med. Chem.* **2010**, *45*, 6077.

[19] R. A. Rowe, M. M. Jones, *Inorg. Synth.* **1957**, *5*, 113.

[20] M. J. Frisch, G. W. Trucks, H. B. Schlegel, G. E. Scuseria, M. A. Robb, J. R. Cheeseman, G. Scalmani, V. Barone, B. Mennucci, G. A. Petersson, H. Nakatsuji, *GAUSSIAN 09, Rev. D.01*, Gaussian, Inc, Wallingford, CT **2009**.

[21] R. D. Dennington II, T.A. Keith, J.M. Millam, GaussView 5.0, *Wallingford, CT*, **2009**

[22] http://www.chemcraftprog.com

[23] G. A. Petersson, A. Bennett, T. G. Tensfeldt, M. A. Al-Laham, W. A. Shirley, J. Mantzaris, *J. Chem. Phys.* **1988**, *89*, 2193.

[24] G. A. Petersson, M. A. Al-Laham, *J. Chem. Phys.* **1991**, *94*, 6081.

[25] P. J. Hay, W. R. Wadt, *J. Chem. Phys.* **1985**, *82*, 299.

[26] A. D. Becke, *J. Chem. Phys.* **1993**, *98*, 5648.

[27] C. Lee, W. Yang, R. G. Parr, *Phys. Rev. B* **1988**, *37*, 785.

[28] R. G. Parr, R. A. Donnelly, M. Levy, W. E. Palke, *J. Chem. Phys.* **1978**, *68*, 3801.

[29] R. G. Parr, R. G. Pearson, *J. Am. Chem. Soc.* **1983**, *105*, 7512.

[30] G. M. Sheldrick, *SHELXS-97, Program of Crystal Structure Solution*, University of Göttingen, Germany **1997**.

[31] G. Sheldrick, *Acta Crystallogr. Sect. A* **2008**, *64*, 112.

[32] M. R. Maurya, C. Haldar, S. Behl, N. B. Kamatham, F. Avecilla, *J. Coord. Chem.* **2011**, *64*, 2995.

[33] M. R. Maurya, C. Haldar, A. A. Khan, A. Azam, A. Salahuddin, A. Kumar, J. C. Pessoa, *Eur. J. Inorg. Chem.* **2012**, 2560.

[34] (a)M. R. Maurya, N. Chaudhary, F. Avecilla, P. Adão, J. C. Pessoa, *Dalton Trans.* **2015**, *44*, 1211. (b)M. R. Maurya, N. Chaudhary, F. Avecilla, *Polyhedron* **2014**, *67*, 436. (c) V. K. Singh, A. Maurya, N. Kesharwani, P. Kachhap, S. Kumari, A. K. Mahato, V. K. Mishra, C. Haldar, *J. Coord. Chem.* **2018**, *71*, 520. (d)P. Mahboubi-Anarjan, R. Bikas, H. Hosseini-Monfared, P. Aleshkevych, P. Mayer, *J. Mol. Struct.* **2017**, *1131*, 258.

[35] S. Kumari, A. K. Mahato, A. Maurya, V. K. Singh, N. Kesharwani, P. Kachhap, I. O. Koshevoy, C. Haldar, *New J. Chem.* **2017**, *41*, 13625.

[36] (a)M. R. Maurya, A. Arya, U. Kumar, A. Kumar, F. Avecilla, J. C. Pessoa, *Dalton Trans.* **2009**, 9555. (b)D. Rehder, C. Weidemann, A. Duch, W. Priebsch, *Inorg. Chem.* **1988**, *27*, 584.

[37] (a)M. R. Maurya, A. A. Khan, A. Azam, S. Ranjan, N. Mondal, A. Kumar, F. Avecilla, J. Costa Pessoa, *Dalton Trans.* **2010**, *39*, 1345. (b)M. R. Maurya, A. A. Khan, A. Azam, S. Ranjan, N. Mondal, A. Kumar, J. Costa Pessoa, *Eur. J. Inorg. Chem.* **2009**, 5377.

[38] M. R. Maurya, M. Bisht, F. Avecilla, *J. Mol. Catal. A: Chem.* **2011**, *344*, 18.

[39] T. A. Koopmans, *Physica* **1993**, *1*, 104.

[40] R. Parr, L. Szentpaly, S. Liu, *J. Am. Chem. Soc.* **1999**, *121*, 1922.

[41] (a)M. A. Martínez, J. V. Durazo, K. L. O. Lara, H. S. Ortega, J. C. G. Ruiz, *Z. Anorg. Allg. Chem.* **2013**, *639*, 1166. (b)J. Pisk, D. Agustin, R. Poli, *Molecules* **2019**, *24*, 783.

[42] A. Maurya, N. Kesharwani, P. Kachhap, V. K. Mishra, N. Chaudhary, C. Haldar, *Appl. Organomet. Chem.* **2019**, 33, e5094.

[43] M. R. Maurya, N. Chaudhary, F. Avecilla, I. Correia, *J. Inorg. Biochem.* **2015**, *147*, 181.

[44] Z. R. Tshentu, C. Togo, R. S. Walmsley, *J. Mol. Catal. A: Chem.* **2010**, *318*, 30.

[45] A. S. Ogunlaja, W. Chidawanyika, E. Antunes, M. A. Fernandes, T. Nyokong, N. Torto, Z. R. Tshentu, *Dalton Trans.* **2012**, *41*, 13908.

[46] R. S. Walmsley, A. S. Ogunlaja, M. J. Coombes, W. Chidawanyika, C. Litwinski, N. Torto, T. Nyokong, Z. R. Tshentu, *J. Mater. Chem.* **2012**, *22*, 5792.

[47] N. D. Chasteen, in *Biological Magnetic Resonance*, (Ed: J. Reuben), Plenum, New York **1981** 53.

[48] D. Rehder, *ioinorganic Vanadium Chemistry*, Wiley & Sons, New York **2008**.

[49] A. G. J. Ligtenbarg, R. Hage, B. L. Feringa, *Coord. Chem. Rev.* **2003**, *237*, 89.

[50] M. R. Maurya, A. A. Khan, A. Azam, A. Kumar, S. Ranjan, N. Mondal, J. C. Pessoa, *Eur. J. Inorg. Chem.* **2009**, *35*, 5377.

[51] M. R. Maurya, S. Agarwal, C. Bader, D. Rehder, *Eur. J. Inorg. Chem.* **2005**, *1*, 147.

[52] M. R. Maurya, S. Agarwal, C. Bader, M. Ebel, D. Rehder, *Dalton Trans.* **2005**, 537.
[53] M. Debnath, M. Dolai, K. Pal, A. Dutta, M. Ali, *Inorg. Chim. Acta* **2018**, *480*, 149.
[54] B. Ghosh, P. Adak, S. Naskar, B. Pakhira, S. K. Chattopadhyay, *Polyhedron* **2017**, *131*, 74.
[55] M. R. Maurya, N. Chaudhary, F. Avecilla, *Polyhedron* **2014**, *67*, 436.
[56] S. Majumder, S. Pasayat, S. Roy, S. P. Dash, S. Dhaka, M. R. Maurya, M. Reichelt, H. Reuter, K. Brzezinski, R. Dinda, *Inorg. Chim. Acta* **2018**, *469*, 366.
[57] G. Grivani, V. Tahmasebi, A. D. Khalaji, *Polyhedron* **2014**, *68*, 144.
[58] P. Adak, B. Ghosh, B. Pakhira, R. Sekiya, R. Kurodab, S. K. Chattopadhyaya, *Polyhedron* **2017**, *127*, 135.
[59] S. K. M. Islam, A. S. Roy, P. Mondal, N. Salam, *J. Mol. Catal. A: Chem.* **2012**, *358*, 38.
[60] R. Khatun, S. Biswas, S. Ghosh, S. K. M. Islam, *J. Organomet. Chem.* **2018**, *858*, 37.
[61] M. R. Maurya, P. Saini, C. Haldar, F. Avecilla, *Polyhedron* **2012**, *31*, 710.
[62] F. M. Collins, A. R. Lucy, C. Sharp, *J. Mol. Catal. A: Chem.* **1997**, *117*, 397.
[63] I. V. Babich, J. A. Moulijn, *Fuel* **2003**, *82*, 607.
[64] G. Romanowski, J. Kira, *Polyhedron* **2017**, *134*, 50.
[65] N. Moussa, J. M. Fraile, A. Ghorbel, J. A. Mayoral, *J. Mol. Catal. A: Chem.* **2006**, *255*, 62.
[66] F. X. Z. Fu, S. Z. Z. Ye, X. Zhou, F. Liu, C. Rong, L. Mao, D. Yin, *J. Mol. Catal. A: Chem.* **2009**, *307*, 93.
[67] R. S. Walmsley, C. Litwinski, E. Antunes, P. Hlangothi, E. Hosten, C. McCleland, T. Nyokong, N. Torto, Z. R. Tshentu, *J. Mol. Catal. A: Chem.* **2013**, *379*, 94.
[68] M. Fadhli, I. Khedher, J. M. Fraile, *J. Mol. Catal. A: Chem.* **2015**, *410*, 140.

## SUPPORTING INFORMATION

Additional supporting information may be found online in the Supporting Information section at the end of this article.

**How to cite this article:** Maurya A, Mahato AK, Chaudhary N, et al. Synthesis and characterization of dimeric μ-oxidovanadium complexes as the functional model of vanadium bromoperoxidase. *Appl Organometal Chem*. 2020;e5508. https://doi.org/10.1002/aoc.5508